

1 **Reply to Reviewer's comments.**

2 I am grateful to the reviewer for very useful and valuable comments and suggestions. They help to  
3 improve substantially the quality of manuscript.

4  
5 The following revisions have been done in according to the comments (colored by blue in the text):

6

7

8 **Comment 1**

9 *In lines 27 – 28, a brief description of the outer Van Allen radiation belt is provided where this population*  
10 *of charged particles is presented as part of the outer magnetosphere, contrary to what has been widely*  
11 *established and is presented in the following publications:*

12 - Baker (1995), *The inner magnetosphere: A review, Surveys in Geophysics*, doi: 10.1007/BF01044572

13 - Ebihara & Miyoshi (2011), *Dynamic inner magnetosphere: A tutorial and recent advances*,  
14 *in Liu W., Fujimoto M. (eds) The dynamic magnetosphere*, doi: 10.1007/978-94-007-0501-2\_9

15

16 **Reply 1**

17 The sentences were revised accordingly:

18 “The outer radiation belt (ORB) is populated by energetic and relativistic electrons trapped in the  
19 magnetosphere at drift shells above  $L \sim 3$  (e.g. Ebihara and Miyoshi, 2011). The ORB is very  
20 dynamic and exhibits variations...”

21 The term “outer magnetosphere” has been removed from whole the text.

22

23

24 **Comment 2**

25 *Additional references on the long-term variations of the radiation belts' structure that should be considered*  
26 *are the following:*

27 - Fung et al. (2006), *Long-term variations of the electron slot region and global radiation belt structure*,  
28 *Geophysical Research Letters*, doi: 10.1029/2005GL024891

29 - Baker & Kanekal (2008), *Solar cycle changes, geomagnetic variations, and energetic particle properties*  
30 *in the inner magnetosphere, Journal of Atmospheric and Solar-Terrestrial Physics*, doi:  
31 10.1016/j.jastp.2007.08.031

32 - Glauert et al. (2018), *A 30-year simulation of the outer electron radiation belt, Space Weather*, doi:  
33 10.1029/2018SW001981

34

35 *On lines 30 and 35, the semi-annual variation of the outer radiation belt is mentioned. This seasonal and*  
36 *not annual change could be explained by the IMF-effect also known as Russell-McPherron effect which is*  
37 *described in:*

38 - Russell & McPherron (1973), *Semiannual variation of geomagnetic activity, Journal of Geophysical*  
39 *Research*, doi: 10.1029/JA078i001p00092

40 - McPherron et al. (2009), *Role of the Russell-McPherron effect in the acceleration of relativistic electrons*,  
41 *Journal of Atmospheric and Solar-Terrestrial Physics*, doi: 10.1016/j.jastp.2008.11.002

42 *and where origins of the seasonal variability in geomagnetic activity have been traced.*

43

44 Reply 2

45 The first paragraph of Introduction section has been revised accordingly:

46 “The ORB is very dynamic and exhibits variations in a wide temporal range: short-term storm-time  
47 and local time variations, 27-day solar rotation, [seasonal](#) and solar cycle variations (e.g. Li et al.,  
48 2001; [Baker and Kanekal, 2008](#); Miyoshi and Kataoka, 2011). During magnetic storms, the ORB is  
49 substantially disturbed and shifted earthward (Baker et al., 2016; Shen et al., 2017). The storm-time  
50 variation is the strongest one for both the ORB location and intensity ([Baker and Kanekal, 2008](#)).  
51 [Magnetic storms produced by interplanetary coronal mass ejecta \(ICME\) and high-speed streams](#)  
52 [\(HSS\) of the solar wind from coronal holes. The seasonal variations with maxima at equinoxes can](#)  
53 [be explained by the effect of interplanetary magnetic field \(IMF\) orientation relative to the](#)  
54 [geomagnetic dipole \(Li et al., 2001; McPherron et al., 2009\). ORB manifests prominent variations](#)  
55 [with the solar cycle \(Fung et al., 2006; Baker and Kanekal, 2008\). It was shown that the maximum](#)  
56 [of ORB is mostly distant from the Earth in solar minimum \(Miyoshi et al., 2004\) and it is closest to](#)  
57 [the Earth during solar maxima \(Glauert et al., 2018\).”](#)

58

59

60 Comment 3

61 *There are minor issues with English language use and several typographical errors.*

62 *For example, on line 54, the term auroral electrojet is first introduced that should be one word. Since Smith*  
63 *et al. (2017) studied both current in the north and south hemisphere, it should also be plural (auroral*  
64 *electrojets – AEJs).*

65

66 Reply 3

67 Corrected

68

69

70 Comment 4

71 *Further down on the same page, on line 72, the work of Kataoka et al. (2015) is listed among the references*  
72 *for the October-November 2003 superstorms although it is focused on the magnetic storm of 17 March*  
73 *2015 which is mentioned further down, in lines 74-81. It should, therefore, be moved more appropriately*  
74 *further down after the brief description of the 2015 Saint Patrick’s Day storm.*

75

76 Reply 4

77 Thank you for suggestion. Corrected.

78

79

80 Comment 5

81 *On line 89, it is indicated that the satellite observations used for the study of the outer electron belt location*  
82 *cover the time period from 1998 to 2016. However, the dates listed in Table 2 are within the time period*

83 *between 2001 and 2018 which is also the time period on which this study is focused as indicated throughout*  
84 *the manuscript.*

85

86 Reply 5

87 The year 1998 is replaced with 2001

88

89 Comment 6

90 *On line 119, it should read “geomagnetic activity was very weak” and not “very week”.*

91

92 Reply 6

93 Corrected

94

95

96 Comment 7

97 *On line 135, it is indicated that Figure 2 shows POES observations from 3 June 2016, while the figure*  
98 *caption indicated that the observations shown are from 2 June 2016.*

99

100 Reply 7

101 Yes, it was misprinting. In Figure 2 caption, 2 June was replaced with 3 June.

102

103

104 Comment 8

105 *In lines 123-126, the close link between increases in solar wind speed and enhancements in electron fluxes*  
106 *in the outer radiation belt is briefly described. Periodic oscillations in the Earth’s magnetic field with*  
107 *frequencies in the range of a few millihertz (ultralow frequency waves) may indeed be an intermediary*  
108 *through which solar wind influences radiation belt dynamics due to their potential for resonant interactions*  
109 *with energetic electrons causing the radial migration of resonant electrons. It should, however, be corrected*  
110 *that electrons are accelerated and increase their energy when they are transported earthward to regions of*  
111 *stronger geomagnetic field. Recent, representative publications on this acceleration mechanism are the*  
112 *following:*

113 *- Mann et al. (2013), Discovery of the action of a geophysical synchrotron in the Earth’s Van Allen radiation*  
114 *belts, Nature Communications, doi: 10.1038/ncomms3795*

115 *- Su et al. (2015), Ultra-low frequency wave-driven diffusion of radiation belt relativistic electrons, Nature*  
116 *Communications, doi: 10.1038/ncomms10096*

117 *Radial transport acts as a loss mechanism when particle drift outward and are lost to the magnetopause.*

118 *The work of Horne et al. (2007) and Reeves et al. (2013), provided as reference, is centered on a different*  
119 *acceleration mechanism acting in the heart of the radiation belt (local acceleration) that involves whistler*  
120 *mode chorus waves rather than waves generated through the Kelvin-Helmholtz instability along the*  
121 *magnetopause.*

122

123 Reply 8

124 Thank you for very useful papers. Note that storm-time acceleration and transport of energetic electrons in  
125 ORB is not the subject of the present study, which is dealing with quiet days. Hence, this part has been  
126 revised accordingly:

127 “Note that the solar wind with the speed of  $V > 400$  km/s is often associated with HSSs from  
128 coronal holes. Fast solar wind streams initiate the Kelvin-Helmholtz instability at the  
129 magnetopause and also produce recurrent magnetic storms, which are accompanied by  
130 intensification of wave activity in the outer magnetosphere that results in effective acceleration and  
131 radial transport of the ORB electrons (Engebretson et al., 1998; Tsurutani et al., 2006; Horne et al.,  
132 2007; Su et al., 2015).”

133

134

135 Comment 9

136 *In lines 187-188, the author notes that the inner edge of the outer radiation is defined as the “first*  
137 *high-latitude point of electron flux enhancements”. Could the latitude above which the flux enhancement*  
138 *was searched be indicated? In addition, which criterion was applied on flux measurements to determine*  
139 *which fluctuations in electron flux correspond to the enhancement observed at the inner edge of the outer*  
140 *electron belt?*

141

142 Reply 9

143 This important issue is described in more details in the revised manuscript:

144 “Apparently, the electron flux enhancements peak in the maximum of ORB. Hence, the inner edge  
145 of ORB corresponds to the beginning of continuous increase of the electron flux from the  
146 minimum at low latitudes to the ORB maximum. This criterion allows determining of the inner  
147 edge for the electrons with energies  $>300$  keV and in the European sector, where the slot region is  
148 not so obvious. Geographic latitude of the inner edge is determined for each year with the accuracy  
149 varying from  $0.5^\circ$  to  $1^\circ$ . In the American sector, the inner edge of ORB is situated at lowest  
150 latitudes from  $43^\circ$  to  $51^\circ$ , in the European sector – from  $55^\circ$  to  $63^\circ$ , and in the Siberian sector – at  
151 highest latitudes from  $58^\circ$  to  $65^\circ$ .”

152

153

154 Comment 10

155 *On line 203, the maximum of solar cycle 23 is indicated that it was observed in 2001 and that of solar cycle*  
156 *24 in 2012-2013. It is not clear to me, and perhaps the reader, how this maximum was defined as both solar*  
157 *cycles were double-peaked according to the number of sunspots observed on the surface of the Sun that has*  
158 *been presented in Figures 4 and 5 with the solid grey line.*

159

160 Reply 10

161 Solar maximum, as a physical phenomenon of the solar magnetic field reversal, has the double-peak  
162 structure both in the 23<sup>rd</sup> and 24<sup>th</sup> solar cycles. Those cycles peaked, respectively, in November 2001 and in  
163 April 2014. After the peaks, the declining phases started and the solar activity was quickly decreasing.  
164 Dramatic changes in the solar magnetic field (including the reversals) were observed from 2000 to 2001 and

165 from 2012 to the beginning of 2014, respectively. In this sense, the maximal phases of those cycles occurred  
166 definitely in 2001 - 2002 and 2012 - 2013. The year of 2014 belongs both to the maximum and to the  
167 declining phase of the 24<sup>th</sup> solar cycle.

168 In the original paper, the year 2000 was not shown and, hence, it was mentioned.

169 In the revised manuscript, this issue is described in more details:

170 “Note that the maximum phases of the 23<sup>rd</sup> and 24<sup>th</sup> solar cycles occurred in the years 2000 - 2001  
171 and in 2012 – April 2014, respectively. The years 2008 – 2009 are the solar minimum phase. The  
172 declining phases lasted from 2003 to 2007 and from 2014 to 2018. In Figures 4 and 5, one can see  
173 that during the declining phase of the current 24<sup>th</sup> solar cycle (especially in the years 2016 – 2018),  
174 the behavior of the ORB maximum and inner edge is different from that during the declining phase  
175 of the previous 23<sup>rd</sup> solar cycle. Namely, their latitudes increased only slightly or even decreased  
176 above North America and especially above Siberia.”

177

178

179 Comment 11

180 *Further down, in the paragraph starting with line 208, an example of how the IGRF-12 model was used on*  
181 *the geographic coordinates of the outer radiation belt maximum flux to obtain the corresponding*  
182 *geomagnetic coordinates is provided. What height was selected as input to the model to determine the*  
183 *geomagnetic or geographic coordinates?*

184

185 Reply 11

186 The height of POES orbit at 850 km was used. Actually for a given magnetic coordinates, the long-term  
187 changes in geographic latitudes predicted by the IGRF-12 model do not vary much with the heights for the  
188 low-earth orbits and ground (10% of the Earth’s radius). The latitudes are different, but their changes with  
189 time are almost same.

190

191

192 Comment 12

193 *The choice of a simple linear fit over the set of outer radiation belt latitudes that have been calculated for*  
194 *the selected quiet days in the period 2001-2018 and are presented in Figures 4 and 5 puzzles me as it seems*  
195 *inadequate to support the main conclusion of the study. There is significant variability in the outer radiation*  
196 *belt location that is related to the solar activity variability that has not been accounted for – although it*  
197 *should - during linear regression.*

198

199 Reply 12

200 The using of linear fit can be justified in the following way:

201 “Unfortunately, there is no any model of the ORB location variation with the solar cycle because  
202 the driving mechanisms are not well established.

203 As a first approach, the variations of ORB location with years are considered as random and can be  
204 fitted by a linear function (indicated by dashed strait lines in Figures 4 and 5):

205 
$$\lambda = a * \text{year} + b, (1)$$

206 where  $\lambda$  is the latitude of maximum or inner edge of ORB. The slope  $a$ , parameter  $b$  and their  
207 standard errors are calculated from a linear regression for various longitudinal regions and various  
208 energies of electrons. The results are presented in Tables 3 and 4 for the ORB maximum and the  
209 inner edge, respectively.”

210  
211 Further  
212 “As one can see in Figures 4 and 5, the long-term variation in IGRF-12 is almost linear function of  
213 the year and, hence, this variation can be easily compared with the linear fits of the ORB location.”  
214

215  
216 Comment 13

217 *The difference in the variability observed in the location of the inner edge of the outer radiation belt or the*  
218 *location of the maximum electron flux has also not been quantified nor considered in the evaluation of the*  
219 *difference estimated between electron observations and magnetic field predictions from the IGRF-12.*

220  
221 Reply 13

222 An effort of inter comparison between the ORB inner edge and maximum was made in the original paper:  
223 “As can be seen in Figures 4 and 5, the location of ORB manifests the well-known solar cycle  
224 variation: the latitudes of ORB maximum and inner edge have a tendency to be highest around  
225 solar minimum in 2008 – 2009 and lowest during solar maxima in the years 2001 and 2012 –  
226 2013.”

227 In the revised manuscript, the difference is quantified and discussed for each longitudinal sector. For  
228 example:

229 “Similar pattern can be found for the inner edge of ORB in the Siberian sector (see Figure 5c).  
230 Namely, the IGRF model predicts a decrease of  $\sim 1^\circ$ . The inner edge was shifted toward lower  
231 latitudes by  $\sim 3^\circ$ ,  $\sim 2^\circ$  and  $\sim 1^\circ$ , respectively, for  $>30$  keV,  $>100$  keV and  $>300$  keV electrons. From  
232 Table 4, one can see that the slope  $a$  is calculated with errors of  $\sim 30\%$  and  $\sim 20\%$ , respectively, for  
233  $>30$  keV and  $>100$  keV electrons. It means that the decrease in latitude might be  $\sim 2^\circ$  (instead of  
234  $\sim 3^\circ$ ) and  $\sim 1.5^\circ$  (instead of  $\sim 2^\circ$ ), respectively. These values are again larger than  $1^\circ$  of the model  
235 prediction. Hence, there is a tendency that the change in the latitudinal location of ORB maximum  
236 is underestimated by the model. This fact indicates that during 17 years from 2001 to 2018, ORB is  
237 abnormally displaced toward the lower latitudes in the Siberian sector.”

238  
239  
240 Comment 14

241 *On line 264, among the reference provided for the effect of the tilt angle variation on the location of the*  
242 *outer radiation belt, the study of Newell et al. (2006) is found. The specific study was centred on the cusp*  
243 *location as it is detailed in the next paragraph and should, therefore, be excluded from the reference list*  
244 *provided here.*

246 Reply 14

247 Corrected, the reference has been replaced.

248

249

250 Comment 15

251 *In lines 269 and 270, the cusp location is suggested as a proxy of the outer radiation boundary. The author*  
252 *must imply the outer edge of the electron radiation belt or more correctly that a displacement of the cusp*  
253 *influences the location of the outer radiation belt but this is not clear from the text. It is also not*  
254 *substantiated by the findings of Newell et al. (2006).*

255 *To date, the inner edge of the outer radiation belt has been suggested to be defined by the plasmopause, the*  
256 *outer boundary of the plasmasphere. Specifically, in the following publication:*

257 *- Baker et al. (2014), Impenetrable barrier to ultrarelativistic electrons in the Van Allen radiation belts,*  
258 *Nature, doi: 10.1038/nature13956 the authors analysed 20 months of electron flux data from the NASA/Van*  
259 *Allen Probes to identify a barrier in the inward transport of ultrarelativistic electron transport.*

260 *Earlier, - Darrouzet et al. (2013), Links between the plasmopause and the radiation belt boundaries as*  
261 *observed by the instruments CIS, RAPID and WHISPER onboard Cluster, Journal of Geophysical Research,*  
262 *doi: 10.1002/jgra.50239*

263 *had reached a different conclusion. The radiation belt location was found to be dependent on the energy*  
264 *range of particles examined but also that the plasmopause is more variable than the inner edge of the outer*  
265 *radiation belt. Namely, the inner or outer edge of the outer electron belt does not always coincide with the*  
266 *plasmopause.*

267

268 Reply 15

269 Thank you very much for very useful papers.

270 This paragraph has been revised accordingly:

271 “The effect of solar wind parameters, including IMF  $B_z$  and dynamic pressure ( $P_d$ ), to the ORB  
272 location is not obvious. It is found that the slot region location can be related to the plasmopause  
273 but the relation is ambiguous (Darrouzet et al., 2013; Baker et al., 2014). We can make indirect  
274 estimation of the effect using a dependence of the cusp location from the solar wind parameters  
275 (Kuznetsov et al., 1993; Newell et al., 2006). The equatorward edge of the cusp separates the open  
276 and close magnetic field lines in the dayside magnetosphere. Hence the latitude of the equatorward  
277 edge can be considered as a proxy of the ORB outer edge. In the first approach, we assume that the  
278 effect of solar wind parameters to the ORB location can be represented by the dynamics of the  
279 ORB outer edge or the cusp equatorward edge. It can be shown that  $B_z = -4$  nT results in less than  
280  $0.5^\circ$  equatorward shift of the cusp and a change of  $P_d$  from 1 to 2 nPa results in  $\sim 0.2^\circ$  decrease in  
281 the latitude of the cusp equatorward edge. Hence, the effects of both  $P_d$  and IMF  $B_z$  are several  
282 times weaker than the difference of  $3^\circ$ .”

283

284

285 Comment 16

286 *In lines 274 and 275, the statement “Variations of the ORB location from cycle to cycle are not investigated*

287 *yet” is not entirely correct. There are indeed significant limitations in such studies due to the lack of data*  
288 *covering several years that could be discussed at this point. Reference to studies such as Glauert et al.*  
289 *(2018) could also be provided.*

290  
291 Reply 16

292 Thank you very much for very useful paper. This part was revised accordingly:

293 “Variations of the ORB location from cycle to cycle and during different phases of solar cycles are  
294 still poorly investigated. It was well established that during solar minima and maxima, the ORB is  
295 located, respectively, at highest and lowest latitudes (Miyoshi et al., 2004; Glauert et al., 2018).  
296 From these findings, we can speculate that lower(higher) solar activity results in an increase (a  
297 decrease) of the ORB latitudes.”

298

299

300 Comment 17

301 *On line 295, the findings of Finlay et al. (2015) suggesting rapid changes in the geomagnetic field in the*  
302 *past 15 years are briefly mentioned. Although the latest change observed in 2012-2013 seems to influence*  
303 *the location of the outer radiation belt, is there a signature of the change observed in 2006 and 2009 in the*  
304 *POES measurements from the same period analysed here?*

305

306 Reply 17

307 This important issue is clarified in the following manner:

308 “We can assume that the abnormal ORB displacement might be related to the geomagnetic jerks.  
309 Though, there is no prominent change in the ORB location in 2006, one can indicate very high latitude of  
310 ORB in 2009. Note that the jerk in 2009 coincided with the abnormally deep solar minimum and, hence, it  
311 could be hard to distinguish between the two effects. On the other hand, we have found significant change  
312 in the ORB dynamics after 2012 – 2013.”

313

314

315 Comment 18

316 *Individual graphs in Figure 2 are difficult to read because of the dark background colour.*

317 *The font size selected for the x and y axis labels are so small that, even after blowing them up to 200%,*  
318 *labels are still difficult to read. On the other hand, titles over the two columns (2016 for the right column*  
319 *and 2006 for the left column) seem to be misplaced.*

320

321 Reply 18

322 Figure 2 has been revised accordingly.

323

324

325 Comment 19

326 *Fonts on plots in Figure 3 could also be enlarged if these are selected to be the final sizes of the graphs.*

327



328 Reply 19

329 The multi-plot Figure 3 is mainly presented in order to demonstrate qualitatively the structure of  
330 ORB and its dynamics in various longitudinal sectors. The results of numerical analysis are  
331 presented in Figures 4 and 5.

332

333

334 **On the radiation belt location in the 23 – 24 solar cycles**

335

336 **Alexei V. Dmitriev<sup>1,2</sup>**

337 <sup>1</sup>Institute of Space Science, National Central University, Jhongli, Taiwan,

338 <sup>2</sup>Skobeltsyn Institute of Nuclear Physics, Lomonosov Moscow State University, Moscow, Russia,

339

340 Corresponding author: Alexei Dmitriev (dalex@jupiter.ss.ncu.edu.tw)

341

342

343 **Abstract**

344 Within the last two solar cycles (from 2001 to 2018), the location of the outer radiation belt (ORB)  
345 was determined with using NOAA/Polar-orbiting Operational Environmental Satellite observations  
346 of energetic electrons with energies above 30 keV. It was found that the ORB was shifted a little  
347 (~1 degrees) in the European and North American sectors while in the Siberian sector, ORB was  
348 displaced equatorward by more than 3 degrees. The displacements corresponded qualitatively to  
349 the change of geomagnetic field predicted by the IGRF-12 model. **However in the Siberian sector,**  
350 **the model has a tendency to underestimate the equatorward shift of ORB.** The shift became  
351 prominent after 2012 that might be related to a geomagnetic jerk occurred in 2012 – 2013. The  
352 displacement of ORB to lower latitudes in the Siberian sector can contribute to an increase in the  
353 occurrence rate of mid-latitude auroras observed in the Eastern Hemisphere.

354

355

356

357 **Keywords:** electron radiation belt, secular geomagnetic variation, mid-latitude aurora

358

## 359 **1. Introduction**

360 The outer radiation belt (ORB) is populated by energetic and relativistic electrons trapped in the  
361 magnetosphere at drift shells above  $L \sim 3$  (e.g. Ebihara and Miyoshi, 2011). The ORB is very  
362 dynamic and exhibits variations in a wide temporal range: short-term storm-time and local time  
363 variations, 27-day solar rotation, seasonal and solar cycle variations (e.g. Li et al., 2001; Baker and  
364 Kanekal, 2008; Miyoshi and Kataoka, 2011). During magnetic storms, the ORB is substantially  
365 disturbed and shifted earthward (Baker et al., 2016; Shen et al., 2017). The storm-time variation is  
366 the strongest one for both the ORB location and intensity (Baker and Kanekal, 2008). Magnetic  
367 storms produced by interplanetary coronal mass ejecta (ICME) and high-speed streams (HSS) of  
368 the solar wind from coronal holes. The seasonal variations with maxima at equinoxes can be  
369 explained by the effect of interplanetary magnetic field (IMF) orientation relative to the  
370 geomagnetic dipole (Li et al., 2001; O'Brien and McPherron, 2002; McPherron et al., 2009). ORB  
371 manifests prominent variations with the solar cycle (Fung et al., 2006; Baker and Kanekal, 2008).  
372 It was shown that the maximum of ORB is mostly distant from the Earth in solar minimum  
373 (Miyoshi et al., 2004) and it is closest to the Earth during solar maxima (Glauert et al., 2018).  
374 Apparently, the intense variations mask relatively weak long-term changes related to a secular  
375 variation of the core and crustal magnetic fields. Recently, a number of authors reported significant  
376 changes in the Earth's magnetic field. The magnetic axial dipole has decreased over the past 175  
377 years by 9% (e.g. Finlay et al., 2016). It was also shown that the north magnetic dip pole, the point  
378 where the magnetic field inclination is vertical, drifted from Canada toward Siberia with the speed  
379 rapidly increasing from 10 km/yr in 1990s to more than 50 km/yr at present (Chulliat et al., 2010;  
380 Thebault et al. 2015). From 1989 to 2002, most dramatic magnetic field changes of  $>50$  nT/yr have  
381 been found in the Canadian Arctic and Eastern Siberia.

382 The effects of dipole decay and pole drift are predicted by International Geomagnetic Reference  
383 Field 12th generation (IGRF-12) model (e.g. Thebault et al. 2015). However in the Siberian sector,  
384 significant anomalies of the main geomagnetic field were found at high latitudes within the  $80^\circ$ - $130^\circ$   
385 longitudinal range (Gvishiani et al., 2014). In this sense, independent verification of changes in the  
386 geomagnetic field at high and middle latitudes is required. Namely, the decrease of magnetic dipole

387 should result in a global equatorward shifting of the magnetospheric domains such as ORB and  
388 auroral region. The drift of the north magnetic pole should cause a decrease(increase) of ORB and  
389 auroral latitudes in the Siberian(North American) sectors.

390 The long-term changes in the location of auroral region were reported by Smith et al. (2017). They  
391 analyzed the latitudinal location of auroral electro jets (AEJs) and revealed a prominent latitudinal  
392 displacement of the AEJs by several degrees in the years 2004 – 2014 relative to the previous solar  
393 maxima in 1970 and 1980. Namely, in the Siberian sector, AEJ shifted to lower latitudes and in the  
394 American sector, AEJ shifted to higher latitudes. The opposite shifts in different sectors cannot be  
395 explained by the solar cycle variation and, thus, it has been attributed to the core and crustal  
396 magnetic fields. On the other hand, the technique of auroral precipitations is hard to use for tracing  
397 of the long-term geomagnetic variations because of high variability in the intensity, location and  
398 extension of aurora (e.g. Cresswell-Moorcock et al., 2013; Smith et al.; 2017).

399 An additional support of prominent changes in the geomagnetic field can be found from a sudden  
400 increase of occurrence of aurora borealis during the years of 2015 to 2017. There were numerous  
401 reports about aurora borealis observed at middle latitudes in the North America, Europe and Russia.  
402 Table 1 lists the days when discrete aurora was detected in big Russian cities Moscow (geographic  
403 location 55°45N 37°37E), St. Petersburg (geographic location 59°57N 30°18E) and Novosibirsk  
404 (geographic location 55°01N 82°55E). It is important to note that while in the North American  
405 region, the mid-latitude discrete aurora is observed quite often, this phenomenon is rare at lower  
406 magnetic latitudes such as in the regions of Central Europe and in particular in Central Russia  
407 (MacDonald et al., 2015; Vázquez et al., 2016). The previous low-latitude aurora borealis was  
408 observed during extremely strong geomagnetic storms with minimum  $Dst < -300$  nT on October -  
409 November 2003 (e.g. Shiokawa et al., 2005; Mikhalev et al., 2004).

410 In contrast, magnetic storms in 2015 – 2017 were not very intense, as one can see in Table 1. The  
411 strongest storm on 17 – 18 March 2015, so-called St. Patrick's Day storm, had minimum  $Dst$  of  
412 -220 nT (e.g. Kataoka et al., 2015). During the St. Patrick's Day storm, aurora borealis was  
413 observed worldwide in North America, Central Europe (e.g. "Strongest geomagnetic storm of  
414 SC24 sparks spectacular aurora display" at <https://watchers.news/2015/03/18/>) and in a number of

415 cities in Central Russia and Siberia (e.g.  
416 <https://www.rt.com/news/241845-aurora-borealis-central-russia/>). Case et al. (2015) found that  
417 during the storm, the discrete aurora was observed at unusually low latitudes, which were much  
418 lower than those predicted by models of Roble and Ridley (1987) and Newell et al. (2010).  
419 The aurora is produced by charged particles precipitating from the magnetosphere to the  
420 high-latitude atmosphere. The charged particles move along the magnetic field lines and, thus, the  
421 location of precipitation is controlled both by the location of source and by the geomagnetic field  
422 configuration. In the present study, we analyze the configuration of the magnetosphere by using  
423 observations of energetic electrons from ORB. At low heights, the ORB electrons are observed at  
424 middle to high latitudes adjacent to the region of auroral precipitations (Lam et al., 2010). Here we  
425 use experimental data on energetic electrons measured by several low-earth orbit (LEO) polar  
426 orbiting satellites during the time period from 2001 to 2016. The method of analysis is described in  
427 section 2. The results are presented and discussed in sections 3 and 4, respectively. Section 5 is  
428 conclusions.

## 429

### 430 **2. Method**

431 Energetic electrons in energy ranges  $>30$  keV,  $>100$  keV and  $>300$  keV are measured at LEO by  
432 the Medium Energy Proton and Electron Detector (MEPED) instruments on board the  
433 NOAA/Polar-orbiting Operational Environmental Satellite (POES) satellites (Evans and Greer,  
434 2004; Asikainen and Mursula 2013). Six POES satellites NOAA-16, NOAA-17, NOAA-18,  
435 NOAA-19, METOP-01 and METOP-02 (hereafter, P6, P7, P8, P9, P1 and P2, respectively) have  
436 Sun-synchronous orbits at altitudes of  $\sim 800$ - $850$  km in different local time sectors. Different POES  
437 satellites were operating during different years as shown in Table 2.

438 The outer magnetosphere and ORB are very dynamic regions, which are directly controlled by  
439 highly variable solar wind plasma streams and interplanetary magnetic field (IMF). As a result, the  
440 location of ORB and its high-latitude projection to the heights of LEO vary substantially (e.g.  
441 Dmitriev et al., 2010; Rodger et al., 2010). Namely, a strong local time variation is related to the  
442 global day-night asymmetry of the magnetosphere such that ORB is observed at higher latitudes

443 during daytime. Variation of geomagnetic tilt angle also causes a change of the ORB latitudinal  
444 location. Interplanetary and geomagnetic disturbances result in a prominent equatorward shift of  
445 ORB.

446 In order to eliminate the disturbing factors, we consider so-called quiet days. Figure 1  
447 demonstrates an example of geomagnetic conditions and measurements of the solar wind plasma  
448 and IMF acquired from Wind upstream monitor during quiet day on 23 June 2006. At that day, the  
449 solar wind velocity was slow ( $\sim 310$  km/s), solar wind dynamic pressure was slightly varying about  
450  $\sim 1.6$  nPa, IMF had northward orientation that resulted in very quiet geomagnetic activity ( $AE <$   
451  $100$  nT,  $Dst \sim 0$  nT).

452 The list of quiet days selected in the time interval from 2001 to 2018 is presented in Table 2. The  
453 solar wind data were acquired from Wind upstream monitor. The selection of quiet days was based  
454 on the following criteria:

455 1. The  $Dst$  variation was close to 0 and  $AE$  index was smaller than 200 nT, i.e. the geomagnetic  
456 activity was very [weak](#).

457 2. The solar wind dynamic pressure  $Pd$  varied slightly around its average values falling in the  
458 range from  $\sim 1$  to 2 nPa.

459 3. The solar wind speed was  $< 400$  km/s and the amplitudes of negative IMF  $B_z$  were weak ( $< 4$  nT).

460 [Note that the solar wind with the speed of  \$V > 400\$  km/s is often associated with HSSs from](#)  
461 [coronal holes. Fast solar wind streams initiate the Kelvin-Helmholtz instability at the](#)  
462 [magnetopause and also produce recurrent magnetic storms, which are accompanied by](#)  
463 [intensification of wave activity in the outer magnetosphere that results in effective acceleration and](#)  
464 [radial transport of the ORB electrons \(Engebretson et al., 1998; Tsurutani et al., 2006; Horne et al.,](#)  
465 [2007; Su et al., 2015\).](#)

466 4. The quiet days were chosen as long as possible after magnetic storms such that storm-time  
467 disturbances of ORB had time to relax. Usually, the quiet days occurred after long-lasting recovery  
468 phase of recurrent magnetic storms (Suvorova et al., 2013).

469 The local time variation of ORB latitudinal location was minimized by a choice of narrow LT  
470 sector around noon (from 10 to 14 LT). We chose quiet days around June solstice in order to

471 minimize the tilt angle variations. Note that June of 2003 and 2007 was very disturbed and there  
472 were no quiet days selected for those years.

473 Figure 2 shows an example of NOAA/POES measurements of energetic electrons in geographic  
474 coordinates during the quiet days on 23 June 2006 and 3 June 2016. The geographic maps are  
475 composed from data retrieved over multiple orbits of the NOAA/POES satellites in the noon sector  
476 ( $12 \pm 2$  LT). For each bin of  $3^\circ$  in longitudes and  $0.5^\circ$  in latitudes, we calculate the average flux of  
477 electrons measured by the  $90^\circ$  detector of the MEPED instrument. At high latitudes, the detector  
478 observes trapped electrons with pitch angles close to  $90^\circ$ , i.e. near the mirror points.

479 The limitation of ORB measurements at given local time is originated from fixed local time of  
480 POES satellites at sun synchronous orbits. As one can see in Figure 2 and Table 2, large statistics  
481 in the Northern hemisphere can be obtained from a number of POES satellites moving in 2-hour  
482 vicinity of local noon around the June solstice. ORB can be easily identified as a wide belt of  
483 intense electron fluxes at high latitudes. At middle latitudes, in longitudinal ranges from  $\sim 90^\circ\text{E}$  to  
484  $180^\circ\text{E}$  in the Eastern Hemisphere and from  $\sim 80^\circ\text{W}$  to  $180^\circ\text{W}$  in the Western Hemisphere, one can  
485 also see intense electron fluxes from the inner electron belt and a slot region between the outer and  
486 inner belts. The slot region is almost vanished in the maps of subrelativistic electrons with energies  
487  $>300$  keV. Qualitative examination of the ORB location in Figure 2 reveals that in the Eastern  
488 Hemisphere, the outer electron belt in 2016 is located few degrees lower in latitudes than that in  
489 the year 2006. Most obvious difference can be found for the slot region, which corresponds to the  
490 low-latitude boundary of ORB.

491 For quantitative determination of the ORB latitudinal displacement, we analyze electron fluxes in  
492  $4^\circ$  vicinities of three longitudes:  $80^\circ\text{W}$  (American sector),  $0^\circ\text{E}$  (European sector) and  $100^\circ\text{E}$   
493 (Siberian sector). Figure 3 shows latitudinal profiles of  $>30$  keV;  $>100$  keV and  $>300$  keV electron  
494 fluxes with pitch angles of  $\sim 90^\circ$  observed by the NOAA/POES satellites around given longitudes  
495 during the quiet days in the years from 2001 to 2018. One can easily identify the maximum of  
496 ORB at high latitudes and the slot region at middle latitudes for the American and Siberian sectors.  
497 Above the Europe, the slot region is not detected at altitudes of the NOAA/POES orbit.

498 It should be noted that after the year 2014, the experimental data on electrons detected by POES is

499 presented in a different format such that the energy channels of electrons are different from those  
500 presented earlier: >40 keV instead of >30 keV, >130 keV instead of >100 keV, and >290 keV  
501 instead of >300 keV. Because of that cross-calibration of the electron detectors is difficult. On the  
502 other hand, the difference in energies is not very large and, thus, it should not affect strongly the  
503 location of ORB. At least the differences are much smaller than the steps between the channels.  
504 Therefore, the complex analysis of all three electron channels allows minimization of this effect.

505

### 506 **3. Results**

507 In Figure 3, the ORB maxima in the American, European and Siberian sectors can be found in the  
508 ranges of latitudes from 50° to 58°, from 64° to 70° and from 62° to 74°, respectively. We  
509 determine geographic latitude of the maxima for each year with the accuracy of 0.5° to 1°. One can  
510 see that the location as well as the intensity of the maximum varies from year to year. The intensity  
511 is minimal during the solar minimum in 2009. The fluxes of >300 keV electrons (Figure 3c) were  
512 very weak such as determination of the ORB was very difficult. In addition, the ORB maximum  
513 above Siberia could not be determined in 2011 because of limited statistics.

514 Qualitatively, the position of ORB maximum above Siberia is more close to 70° and 65°,  
515 respectively, in 2001 - 2010 and in 2012 – 2018. Above the Europe and North America, variation  
516 of the ORB location is more random. The fluxes of >30 keV electrons in the outer region of ORB  
517 are very dynamic because of strong contribution from the auroral population. The latter produced  
518 additional maxima at latitudes above 70° and 55°, respectively, in the European-Siberian and  
519 American sectors. The additional maxima were very intense in the years 2008, 2010 and 2017 that  
520 made difficult to determine the actual location of the ORB. In those cases, we chose the maximum  
521 located at lower latitude. This choice gives a good agreement with the ORB maximum location for  
522 the >100 keV electrons and especially subrelativistic >300 keV electrons, which are practically  
523 free from the auroral contamination.

524 In Figure 3, one can clearly see the slot region between the outer and inner electron belts in the  
525 latitudinal ranges 45° - 50° and 45° - 50° above North America and Siberia, respectively. This  
526 structure can be well identified and numerically determined, excepting >300 keV electrons. We



527 determine the first high-latitude point of electron flux enhancements as the low-latitude edge of  
528 ORB. Apparently, the electron flux enhancements peak in the maximum of ORB. Hence, the inner  
529 edge of ORB corresponds to the beginning of continuous increase of the electron flux from the  
530 minimum at low latitudes to the ORB maximum. This criterion allows determining of the inner  
531 edge for the electrons with energies  $>300$  keV and in the European sector, where the slot region is  
532 not so obvious. Geographic latitude of the inner edge is determined for each year with the accuracy  
533 varying from  $0.5^\circ$  to  $1^\circ$ . In the American sector, the inner edge of ORB is situated at lowest  
534 latitudes from  $43^\circ$  to  $51^\circ$ , in the European sector – from  $55^\circ$  to  $63^\circ$ , and in the Siberian sector – at  
535 highest latitudes from  $58^\circ$  to  $65^\circ$ . In Figure 3, one can find that the latitude of ORB edge above  
536 Siberia decreases with years from  $\sim 65^\circ$  to  $60^\circ$  for all energy range of electrons. The change of  
537 ORB location above the Europe and North America is not so obvious.

538 Figures 4 and Figure 5 show long-term variations in the location of ORB and corresponding  
539 predictions of the IGRF-12 model during 17 years from 2001 to 2018. As one can see, the ORB  
540 maximum and inner edge of  $>30$  keV electrons are usually located at higher latitudes than those of  
541  $>100$  keV electrons, and the ORB of subrelativistic  $>300$  keV electrons is located at lowest  
542 latitudes. Note that the location of ORB maximum for  $>30$  keV electrons is scattered significantly  
543 and it is different from those for the more energetic electrons because of substantial contamination  
544 from the auroral electrons. In contrast, the ORB maxima and inner edge of  $>100$  keV and  $>300$   
545 keV electrons demonstrate very similar dynamics.

546 As can be seen in Figures 4 and 5, the location of ORB manifests the well-known solar cycle  
547 variation: the latitudes of ORB maximum and inner edge have a tendency to be highest around  
548 solar minimum in 2008 – 2009 and lowest during solar maxima in the years 2001 and 2012 – 2013.  
549 Note that the maximum phases of the 23<sup>rd</sup> and 24<sup>th</sup> solar cycles occurred in the years 2000 - 2001  
550 and in 2012 – April 2014, respectively. The years 2008 – 2009 are the solar minimum phase. The  
551 declining phases lasted from 2003 to 2007 and from 2014 to 2018. In Figures 4 and 5, one can see  
552 that during the declining phase of the current 24<sup>th</sup> solar cycle (especially in the years 2016 – 2018),  
553 the behavior of the ORB maximum and inner edge is different from that during the declining phase  
554 of the previous 23<sup>rd</sup> solar cycle. Namely, their latitudes increased only slightly or even decreased

555 above North America and especially above Siberia. Unfortunately, there is no any model of the  
556 ORB location variation with the solar cycle because the driving mechanisms are not well  
557 established.

558 As a first approach, the variations of ORB location with years are considered as random and can be  
559 fitted by a linear function (indicated by dashed strait lines in Figures 4 and 5):

$$560 \quad \lambda = a * \text{year} + b, (1)$$

561 where  $\lambda$  is the latitude of maximum or inner edge of ORB. The slope  $a$ , parameter  $b$  and their  
562 standard errors are calculated from a linear regression for various longitudinal regions and various  
563 energies of electrons. The results are presented in Tables 3 and 4 for the ORB maximum and the  
564 inner edge, respectively.

565 The linear fits are compared with geomagnetic field trends predicted by the IGRF model in  
566 different regions. The trends were calculated in the following manner. First, we took a point with  
567 given geographic coordinates and calculated its magnetic coordinates for the quiet day on 29 June  
568 2001 using the IGRF model of epoch 2000. Namely, for the ORB maximum, we took points (70°N,  
569 80°W), (66°N, 0°E) and (54°N, 100°E), respectively, for the American, European and Siberian  
570 sectors and calculated their geomagnetic coordinates (64.12°N, 11.44°W), (67.05°N, 95.66°E) and  
571 (59.5°N, 174.3°E), respectively. For the inner edge of ORB, we took, respectively, (46.5°N, 80°W),  
572 (59°N, 0°E) and (63°N, 100°E), with corresponding geomagnetic coordinates (56.62°N, 10.61°W)  
573 (60.59°N, 89.34°E) and (52.47°N, 173.7°E). Then we supposed that the geomagnetic coordinates  
574 of the points do not change with time and we used them to calculate geographic coordinates from  
575 the IGRF-12 model for corresponding quiet days listed in Table 2. The geographic coordinates of a  
576 point with given magnetic coordinates should be changed with time because of long-term variation  
577 of the geomagnetic field. As one can see in Figures 4 and 5, the long-term variation in IGRF-12 is  
578 almost linear function of the year and, hence, this variation can be easily compared with the linear  
579 fits of the ORB location.

580 In the American sector (see Figure 4a), the latitude of ORB maximum demonstrates a little  
581 decrease of about 1° while the IGRF-12 model predicts an increase of ~1°. The decrease results  
582 from relatively low latitudes, where the ORB maximum is located from 2013 to 2018. The location

583 of inner edge of ORB in the American sector (see Figure 5a) does not practically change within the  
584 experimental uncertainty of  $\sim 1^\circ$ . Note that in both cases, the slope  $a$  has very large error (see  
585 Tables 3 and 4). The errors are comparable or even exceed the values of slope. Hence, from the  
586 statistical consideration one can conclude that the model prediction does not contradict to the  
587 observations.

588 In the European sector (Figures 4b and 5b), the IGRF-12 model predicts very small change of  $0.3^\circ$   
589 in the ORB location that is in good agreement with the ORB maximum dynamics. The location of  
590 ORB inner edge for electrons with energies  $>30$  keV and  $>100$  keV demonstrates an increase of  
591  $\sim 3^\circ$ . However, the slope of increase is determined with a substantial error of up to 50% (see Table  
592 4) that produces an increase by only  $\sim 1.5^\circ$ . In addition, the  $>300$  keV electrons follow the model  
593 and do not exhibit any prominent trend. Hence in the European sector, the IGRF model predicts the  
594 ORB dynamics with sufficient accuracy.

595 in the Siberian sector, the IGRF model predicts  $\sim 1^\circ$  decrease in latitude of the ORB maximum and  
596 inner edge as shown in Figures 4c and 5c. From the POES observations, we find that the ORB  
597 maximum is displaced to lower latitudes by at least  $\sim 3^\circ$  in all electron energy channels: from  $\sim 69^\circ$   
598 to  $\sim 66^\circ$  for  $>300$  keV electrons, from  $\sim 70^\circ$  to  $66^\circ$  for  $>100$  keV electrons and from  $\sim 71^\circ$  to  $67^\circ$  for  
599  $>30$  keV electrons (see Figure 4c). The difference is related to very low latitudes ( $\sim 67^\circ$  and less) of  
600 the ORB maximum during solar maximum and on the declining phase of the current 24th solar  
601 cycle in the years 2012 - 2013 and 2016 - 2018, respectively. In the solar maximum and on the  
602 declining phase of the previous 23rd solar cycle (the years 2001 and 2004 - 2006), the ORB  
603 maximum was located at higher latitudes (above  $67^\circ$ ). Note that the error in determination of the  
604 slope  $a$  is  $\sim 50\%$  as shown in Table 3. Hence statistically, the decrease of latitude might be two  
605 times smaller, i.e.  $\sim 1.5^\circ$  to  $2^\circ$ . This decrease is slightly larger than  $1^\circ$  of the model prediction,  
606 within  $0.5^\circ$  to  $1^\circ$  statistical uncertainty in determination of latitude.

607 Similar pattern can be found for the inner edge of ORB in the Siberian sector (see Figure 5c).  
608 Namely, the IGRF model predicts a decrease of  $\sim 1^\circ$ . The inner edge was shifted toward lower  
609 latitudes by  $\sim 3^\circ$ ,  $\sim 2^\circ$  and  $\sim 1^\circ$ , respectively, for  $>30$  keV,  $>100$  keV and  $>300$  keV electrons. From  
610 Table 4, one can see that the slope  $a$  is calculated with errors of  $\sim 30\%$  and  $\sim 20\%$ , respectively, for

611 >30 keV and >100 keV electrons. It means that the decrease in latitude might be  $\sim 2^\circ$  (instead of  
612  $\sim 3^\circ$ ) and  $\sim 1.5^\circ$  (instead of  $\sim 2^\circ$ ), respectively. These values are again larger than  $1^\circ$  of the model  
613 prediction. Hence, there is a tendency that the change in the latitudinal location of ORB maximum  
614 is underestimated by the model. This fact indicates that during 17 years from 2001 to 2018, ORB is  
615 abnormally displaced toward the lower latitudes in the Siberian sector.

616 It is interesting to point out the year 2017, when the maximum and inner edge of ORB shifted to  
617 very low latitudes of  $62^\circ$  and  $\sim 59^\circ$  respectively. The shift was observed during two quiet days on 9  
618 and 10 June 2017. Similar pattern of displacement can be found on the declining phase of the  
619 previous 23rd solar cycle in the year 2005, when the ORB suddenly shifted equatorward by more  
620 than  $\sim 2^\circ$ . Note that if we exclude the year 2017 from the linear fitting then the results are not  
621 practically changed because ORB is located at relatively low latitudes during the years 2012 to  
622 2018.

623

#### 624 **4. Discussion**

625 We have found up to  $4^\circ$  equatorward displacement of the ORB in the Siberian sector. The  
626 displacement is larger than that predicted by the IGRF-12 model. The difference is statistically  
627 significant. It might result both from a change of the geomagnetic field and from changes of  
628 driving parameters such as geomagnetic activity, the tilt angle, IMF  $B_z$  and solar wind dynamic  
629 pressure. It is well known that those parameters affect the latitudinal location of domains in the  
630 magnetosphere. The effect of geomagnetic activity was eliminated by the choice of quiet days. The  
631 other drivers are considered below.

632 The tilt angle in the noon region at given longitude ( $80^\circ\text{W}$ ,  $0^\circ\text{E}$  and  $100^\circ\text{E}$ ) varies a little ( $<2^\circ$ )  
633 during the June month. The change of local time in 2-hour vicinity of noon produces  $\sim 5^\circ$  variation  
634 of the tilt angle. The tilt angle variations of a few degrees result in a tiny change of  $\sim 0.1^\circ$  in the  
635 ORB latitude (e.g. Dmitriev et al., 2010). Hence, we can neglect the effect of tilt angle.

636 The effect of solar wind parameters, including IMF  $B_z$  and dynamic pressure ( $P_d$ ), to the ORB  
637 location is not obvious. outer magnetosphere domains was comprehensively investigated  
638 (Kuznetsov et al., 1993; Newell et al., 2006;). Namely it was shown a dependence of the cusp

639 low-latitude boundary on the IMF  $B_z$  such that  $B_z = -4$  nT results in less than  $0.5^\circ$  equatorward  
640 shift. The cusp location can be considered as a proxy of the ORB boundary. Similar situation can  
641 be found with the solar wind dynamic pressure: a change of  $P_d$  from 1 to 2 nPa results in  $\sim 0.2^\circ$   
642 decrease in the latitude of the ORB boundary. Hence, the effects of both  $P_d$  and IMF  $B_z$  are  
643 several times weaker than the difference of  $3^\circ$ .

644 Another possible effect is the solar cycle variation. Variations of the ORB location from cycle to  
645 cycle and during different phases of solar cycles are still poorly investigated. It was well  
646 established that during solar minima and maxima, the ORB is located, respectively, at highest and  
647 lowest latitudes (Miyoshi et al., 2004; Glauert et al., 2018). From these findings, we can speculate  
648 that lower(higher) solar activity results in an increase (a decrease) of the ORB latitudes. In Figure  
649 3, one can see that the intensities of electrons are weaker after the beginning of the 24th solar  
650 maximum in 2012 in comparison with the 23rd solar cycle. Note that the 23rd solar cycle was  
651 stronger than the 24th one. Following this logic, the ORB should be located at relatively higher  
652 latitudes during the weak 24th solar cycle than during the strong 23rd solar cycle. However, we  
653 have found totally opposite effect: ORB over Siberia is located at lower latitudes after 2012.

654 From the above, we can conclude that the difference between the observations and predictions can  
655 be rather originated from anomalous dynamics of the geomagnetic field. This idea is supported by  
656 the observations of ORB location over the Europe and North America, where the ORB  
657 displacement is well predicted by the IGRF-12 model. An additional support can be found from  
658 results of long-term magnetic observations in Siberia where significant anomalies of the main  
659 geomagnetic field have been revealed in the  $80^\circ$ - $130^\circ$  longitudinal range (Gvishiani et al., 2014).  
660 Namely, the IGRF-12 model predicted the magnetic field up to 300 nT stronger than that measured  
661 by ground based magnetic stations that was close to 0.5% of the total magnetic field in this region.  
662 For the geodipole, stronger magnetic field corresponds to higher latitudes.

663 In Figures 4c and 5c, one can see that the decrease of ORB latitude in the Siberian sector is most  
664 prominent after 2012. On the other hand in the years 2012 –2013, a sudden change was found in  
665 the acceleration of secular variation in the geomagnetic field (Finlay et al., 2015). Analyzing time  
666 interval from 1999 to 2015, Finlay et al. (2015) revealed 3 pulses in time evolution of the mean

667 square secular acceleration power: in 2006, in 2009 and in 2012 – 2013. Chulliat et al. (2015)  
668 attribute these pulses, or so-called sharp geomagnetic "jerks", to magnetic field variations  
669 originating in the Earth's core. We can assume that the abnormal ORB displacement might be  
670 related to the geomagnetic jerks. We can assume that the abnormal ORB displacement might be  
671 related to the geomagnetic jerks. Though, there is no prominent change in the ORB location in 2006, one  
672 can indicate very high latitude of ORB in 2009. Note that the jerk in 2009 coincided with the abnormally  
673 deep solar minimum and, hence, it could be hard to distinguish between the two effects. On the other hand,  
674 we have found significant change in the ORB dynamics after 2012 – 2013.

675 The several degrees equatorward displacement of ORB in the Siberian sector indicates an  
676 equatorward shifting of all domains in the magnetosphere, including the region of auroral  
677 precipitations. Apparently, the shifting contributes to the increase in occurrence rate of the  
678 mid-latitude auroras in Siberia and, perhaps, in entire Russia. In addition, Finlay et al. (2015)  
679 expect that the next jerk might occur around 2016. We do not have any reports about the recent  
680 jerks yet. But very strong decrease of the ORB latitude observed in 2017 might indicate the sudden  
681 change in the geomagnetic field.

682

## 683 5. Conclusions

684 NOAA/POES observations of electrons with energies of few tens and hundreds of keV allowed  
685 revealing and measure a latitudinal displacement of the outer radiation belt during last 18 years.  
686 The displacement corresponds qualitatively to the change of geomagnetic field predicted by the  
687 IGRF-12 model. However in the Siberian sector, the model has a tendency to underestimate the  
688 equatorward shift of ORB. ~~However, numerically the equatorward shift in the Siberian sector was  
689 found more than  $\sim 2^\circ$  larger than that predicted by the model.~~ The shift became prominent after  
690 2012 that might be related to the geomagnetic jerk occurred in 2012 – 2013. The increase in the  
691 occurrence rate of mid-latitude auroras in the Eastern Hemisphere can be explained, at least  
692 partially, by the equatorward displacement of the high-latitude projection of the magnetosphere  
693 domains.

694

695 **Acknowledgments** The authors thank a team of NOAA's Polar Orbiting Environmental Satellites  
696 for providing experimental data about energetic particles, the CDAWEB for providing the Wind  
697 solar wind data, Kyoto World Data Center for Geomagnetism  
698 (<http://wdc.kugi.kyoto-u.ac.jp/igrf/point/index.html>) for providing the geomagnetic indices and  
699 computation of the IGRF12 model, and WDC-SILSO, Royal Observatory of Belgium, Brussels for  
700 providing sunspot numbers (<http://www.sidc.be/silso/datafiles>). The work was supported by grant  
701 MOST-106-2111-M-008-015-, R&D foundation from National Central University and partially by  
702 grant NSC103-2923-M-006-002-MY3/14-05-92002HHC\_a of Taiwan - Russia Research  
703 Cooperation.  
704

705 **References**

706 Asikainen, T., and Mursula, K.: Correcting the NOAA/MEPED energetic electron fluxes for  
707 detector efficiency and proton contamination, *J. Geophys. Res. Space Physics*, 118,  
708 doi:10.1002/jgra.50584, 2013.

709 Baker, D. N., and Kanekal, S. G.: Solar cycle changes, geomagnetic variations, and energetic  
710 particle properties in the inner magnetosphere, *Journal of Atmospheric and Solar-Terrestrial*  
711 *Physics*, 70, 195–206, doi: 10.1016/j.jastp.2007.08.031, 2008.

712 Baker, D. N. et al.: An impenetrable barrier to ultrarelativistic electrons in the Van Allen radiation  
713 belts, *Nature*, 515, 531 - 534, doi: 10.1038/nature13956, 2014.

714 Baker, D. N., Jaynes, A. N., Kanekal, S. G., Foster, J. C., Erickson, P. J., Fennell, J. F., Blake, J. B.,  
715 Zhao, H., Li, X., Elkington, S. R., Henderson, M. G., Reeves, G. D., Spence, H. E., Kletzing, C.  
716 A., and Wygant, J. R.: Highly relativistic radiation belt electron acceleration, transport, and loss:  
717 Large solar storm events of March and June 2015, *J. Geophys. Res. Space Physics*, 121,  
718 6647-6660, doi:10.1002/2016JA022502, 2016.

719 Case, N. A., MacDonald, E. A., and Patel, K. G.: Aurorasaurus and the St Patrick's Day storm,  
720 *Astronomy & Geophysics* 56(3), 13-14. DOI: 10.1093/astrogeo/atv089, 2015.

721 Chulliat, A., Hulot, G., and Newitt, L. R.: Magnetic flux expulsion from the core as a possible  
722 cause of the unusually large acceleration of the north magnetic pole during the 1990s, *J.*  
723 *Geophys. Res.*, 115, B07101, doi:10.1029/2009JB007143, 2010.

724 Chulliat A., Alken, P., and Maus, S.: Fast equatorial waves propagating at the top of the Earth's  
725 core. *Geophys Res Lett.*, 42(9), 3321-3329, doi:10.1002/2015GL064067, 2015.



726 Cresswell-Moorcock, K., Rodger, C. J., Kero, A., Collier, A. B., Clilverd, M. A., Häggström, I.,  
727 and Pitkänen, T.: A reexamination of latitudinal limits of substorm-produced energetic electron  
728 precipitation, *J. Geophys. Res. Space Physics*, 118, 6694-6705, doi:10.1002/jgra.50598, 2013.

729 Darrouzet, F., Pierrard, V., Benck, S., Lointier, G., Cabrera, J., Borremans, K., Ganushkina, N. Yu.,  
730 and Keyser, J. De.: Links between the plasmopause and the radiation belt boundaries as  
731 observed by the instruments CIS, RAPID and WHISPER onboard Cluster, *J. Geophys. Res.*  
732 *Space Physics*, 118, 4176-4188, doi:10.1002/jgra.50239, 2013.

733 Dmitriev, A. V., Jayachandran, P. T., and Tsai, L.-C.: Elliptical model of cutoff boundaries for the  
734 solar energetic particles measured by POES satellites in December 2006, *J. Geophys. Res.*, 115,  
735 A12244, doi:10.1029/2010JA015380, 2010.

736 Ebihara Y., and Y. Miyoshi (2011): Dynamic inner magnetosphere: A tutorial and recent advances,  
737 in Liu W., Fujimoto M. (eds) *The dynamic magnetosphere*, 145 – 187, doi:  
738 [10.1007/978-94-007-0501-2\\_9](https://doi.org/10.1007/978-94-007-0501-2_9)

739 Engebretson, M., Glassmeier, K.-H., Stellmacher, M., Hughes, W. J., and Luhr, H.: The  
740 dependence of high-latitude Pc5 wave power on solar wind velocity and on the phase of  
741 high-speed solar wind streams, *J. Geophys. Res.*, 103, 26,271-26,283, doi:10.1029/97JA03143,  
742 1998.

743 Evans, D. S., and Greer, M. S.: Polar Orbiting Environmental Satellite Space Environment Monitor:  
744 2. Instrument Descriptions and Archive Data Documentation, Tech. Memo. Version 1.4, NOAA  
745 Space Environ. Lab., Boulder, Colo., 2004.

746 Fung, S. F., Shao, X. and Tan L. C.: Long-term variations of the electron slot region and global

747 radiation belt structure, *Geophys. Res. Lett.*, 33, L04105, doi:10.1029/2005GL024891, 2006.

748 Finlay, C. C., Aubert, J., and Gillet, N.: Gyre-driven decay of the Earth's magnetic dipole, *Nat.*  
749 *Commun*, 7:10422, 1 - 8, doi: 10.1038/ncomms10422, 2016.

750 Glauert, S. A., Horne, R. B., and Meredith, N. P.: A 30-year simulation of the outer electron  
751 radiation belt, *Space Weather*, 16, 1498-1522. <https://doi.org/10.1029/2018SW001981>, 2018.

752 Gvishiani, A., Lukianova, R., Soloviev, A., Khokhlov, A.: Survey of Geomagnetic Observations  
753 Made in the Northern Sector of Russia and New Methods for Analysing Them, *Surv.*  
754 *Geophys.*,35, 1123-1154, DOI 10.1007/s10712-014-9297-8, 2014.

755 Horne, R. B., Thorne, R. M., Glauert, S. A., Meredith, N. P., Pokhotelov, D., and Santolik, O.:  
756 Electron acceleration in the Van Allen radiation belts by fast magnetosonic waves, *Geophys.*  
757 *Res. Lett.*, 34, L17107, doi:10.1029/2007GL030267, 2007.

758 Kataoka, R., Shiota, D., Kilpua, E., and Keika, K.: Pileup accident hypothesis of magnetic storm  
759 on 17 March 2015, *Geophys. Res. Lett.*, 42, 5155-5161, doi:10.1002/2015GL064816, 2015.

760 Kuznetsov, S.N., Suvorova, A.V., and Tolstaya, E.D.: Relationship of the cleft latitude to  
761 interplanetary parameters and DST variations, *Cosmic Research*, 31(4), 409-415 (Translated  
762 from *Kosmicheskie Issledovaniya*), 1993.

763 Lam, M. M., Horne, R. B., Meredith, N. P., Glauert, S. A., Moffat-Griffin, T., and Green, J. C.:  
764 Origin of energetic electron precipitation >30 keV into the atmosphere, *J. Geophys. Res.*, 115,  
765 A00F08, doi:10.1029/2009JA014619, 2010.

766 Li, X., Baker, D. N., Kanekal, S. G., Looper, M., and Temerin, M.: Long term measurements of  
767 radiation belts by SAMPEX and their variations, *Geophys. Res. Lett.*, 28(20), 3827-3830, DOI:

768 10.1029/2001GL013586, 2001.

769 MacDonald, E. A., Case, N. A., Clayton, J. H., Hall, M. K., Heavner, M., Lalone, N., Patel, K. G.,  
770 and Tapia, A.: Aurorasaurus: A citizen science platform for viewing and reporting the aurora,  
771 *Space Weather*, 13, doi:10.1002/2015SW001214, 2015.

772 [McPherron, Baker, D. N., and Crooker, N. U.: Role of the Russell-McPherron effect in the](#)  
773 [acceleration of relativistic electrons, \*Journal of Atmospheric and Solar-Terrestrial Physics\*, 71,](#)  
774 [1032-1044, doi: 10.1016/j.jastp.2008.11.002, 2009.](#)

775 Mikhalev, A. V., Beletsky, A. B., Kostyleva, N. V., and Chernigovskaya, M. A.: Midlatitude  
776 Auroras in the South of Eastern Siberia during Strong Geomagnetic Storms on October 29-31,  
777 2003 and November 20-21, 2003, *Cosmic Research*, 42(6), 591-596 (Translated from  
778 *Kosmicheskie Issledovaniya*, 42(6), 616-621), 2004.

779 Miyoshi, Y. and Kataoka, R.: Solar cycle variations of outer radiation belt and its relationship to  
780 solar wind structure dependences, *Journal of Atmospheric and Solar-Terrestrial Physics*, 73(10),  
781 77-87, doi:10.1016/j.jastp.2010.09.031, 2011.

782 Miyoshi, Y. S., Jordanova, V. K., Morioka, A., and Evans, D. S.: Solar cycle variations of the  
783 electron radiation belts: Observations and radial diffusion simulation, *Space Weather*, 2,  
784 S10S02, doi:10.1029/2004SW000070, 2004.

785 Newell, P. T., Sotirelis, T., Liou, K., Meng, C.-I., and Rich, F. J.: Cusp latitude and the optimal  
786 solar wind coupling function, *J. Geophys. Res.*, 111, A09207, doi:10.1029/2006JA011731,  
787 2006.

788 Newell, P. T., Sotirelis, T., and Wing, S.: Seasonal variations in diffuse, monoenergetic, and

789 broadband aurora, *J. Geophys. Res.*, 115, A03216, doi:10.1029/2009JA014805, 2010.

790 O'Brien, T. P., and McPherron, R. L.: Seasonal and diurnal variation of Dst dynamics, *J. Geophys.*  
791 *Res.*, 107(A11), 1341, doi:10.1029/2002JA009435, 2002.

792 Roble, R. G., and Ridley, E. C.: An auroral model for the NCAR thermospheric general circulation  
793 model (TGCM), *Ann. Geophys.*, 5, 369-382, 1987.

794 Rodger, C. J., Clilverd, M. A., Green, J. C., and Lam, M. M.: Use of POES SEM-2 observations to  
795 examine radiation belt dynamics and energetic electron precipitation into the atmosphere, *J.*  
796 *Geophys. Res.*, 115, A04202, doi:10.1029/2008JA014023, 2010.

797 Shen, X.-C., Hudson, M. K., Jaynes, A., Shi, Q., Tian, A., Claudepierre, S., Qin, M.-R., Zong, Q.-G.,  
798 and Sun, W.-J.: Statistical study of the storm time radiation belt evolution during Van Allen  
799 Probes era: CME- versus CIR-driven storms, *J. Geophys. Res. Space Physics*, 122, 8327-8339,  
800 doi:10.1002/2017JA024100, 2017.

801 Shiokawa, K., Ogawa, T., and Kamide, Y.: Low-latitude auroras observed in Japan: 1999–2004, *J.*  
802 *Geophys. Res.*, 110, A05202, doi:10.1029/2004JA010706, 2005.

803 Smith, A. R. A., Beggan, C. D., Macmillan, S., and Whaler, K. A.: Climatology of the auroral  
804 electrojets derived from the along-track gradient of magnetic field intensity measured by  
805 POGO, Magsat, CHAMP, and Swarm. *Space Weather*, 15,  
806 <https://doi.org/10.1002/2017SW001675>, 2017.

807 Su, Z. et al.: Ultra-low-frequency wave-driven diffusion of radiation belt relativistic electrons, *Nat.*  
808 *Commun.*, 6:10096, doi: 10.1038/ncomms10096, 2015.

809 Suvorova, A. V., Dmitriev, A. V., Tsai, L.-C., Kunitsyn, V. E., Andreeva, E. S., Nesterov, I. A., and

810 Lazutin, L. L.: TEC evidence for near-equatorial energy deposition by 30 keV electrons in the  
811 topside ionosphere, *J. Geophys. Res. Space Physics*, 118, 4672-4695, doi:10.1002/jgra.50439,  
812 2013.

813 Thebault E. et al.: International Geomagnetic Reference Field: the 12th generation, *Earth, Planets*  
814 *and Space*, 67:79, 2 – 19, doi 10.1186/s40623-015-0228-9, 2015.

815 [Tsurutani, B. T., et al.: Corotating solar wind streams and recurrent geomagnetic activity: A review,](#)  
816 [J. Geophys. Res., 111, A07S01, doi:10.1029/2005JA011273, 2006.](#)

817 Vázquez, M., Vaquero, J. M., Gallego, M. C., Roca Cortés, T., Pallé, P. L.: Long-Term Trends and  
818 Gleissberg Cycles in Aurora Borealis Records (1600 - 2015), *Solar Phys* 291, 613-642, DOI  
819 10.1007/s11207-016-0849-6, 2016.

820

821 **Table 1.** Observations of discrete aurora in Russia in the years 2015 to 2016

Date	min Dst, nT	City	Geomagnetic location	Reference
2015 March 17-18	-220	Moscow	51°16N 122°06E	Ref1
2015 June 22-23	-200	Moscow	51°16N 122°06E	Ref2
2015 August 16-17	-84	St. Petersburg	56°23N 117°36E	Ref3
2015 October 7-8	-120	St. Petersburg	56°23N 117°36E	Ref4
2016 February 17-18	-50	St. Petersburg	56°24N 117°37E	Ref5
2016 April 3-4	-50	St. Petersburg	56°24N 117°37E	Ref6
2016 August 24-25	-80	St. Petersburg	56°24N 117°37E	Ref7
2017 September 7-8	-124	Novosibirsk	45°56N 160°07E	Ref8
2017 November 7-8	-74	St. Petersburg	56°25N 117°38E	Ref9

822 Ref1 - [www.dp.ru/a/2015/03/18/Severnoe\\_sijanie\\_uvideli\\_zh/](http://www.dp.ru/a/2015/03/18/Severnoe_sijanie_uvideli_zh/)

823 Ref2 - [www.dp.ru/a/2015/06/23/Severnoe\\_sijanie\\_uvideli\\_v/](http://www.dp.ru/a/2015/06/23/Severnoe_sijanie_uvideli_v/)

824 Ref3 - <http://47news.ru/articles/92419/>

825 Ref4 - [www.dp.ru/a/2015/10/08/Severnoe\\_sijanie\\_v\\_Peterbu/](http://www.dp.ru/a/2015/10/08/Severnoe_sijanie_v_Peterbu/)

826 Ref5 - [www.fontanka.ru/2016/02/17/058/](http://www.fontanka.ru/2016/02/17/058/)

827 Ref6 - [www.dp.ru/a/2016/04/03/ZHiteli\\_Peterburga\\_deljatsja/](http://www.dp.ru/a/2016/04/03/ZHiteli_Peterburga_deljatsja/)

828 Ref7 - [www.fontanka.ru/2016/08/24/035/](http://www.fontanka.ru/2016/08/24/035/) and [www.topnews.ru/news\\_id\\_92986.html](http://www.topnews.ru/news_id_92986.html)

829 Ref8 - <http://www.ntv.ru/video/1515160/>

830 Ref9 - <https://www.fontanka.ru/2017/11/07/134/>

831

832

833 **Table 2.** List of quiet days in June selected for POES observations of the outer radiation belt.

Year	Day in June	Start UT	Duration, hours	V* km/s	Pd** nPa	Bz <sub>min</sub> <sup>§</sup> nT	POES Satellites <sup>#</sup>
2001	29	0	24	350	1.6 (1.0 – 3.2)	0.6 (-4)	P6
2002	28	0	24	340	1.2 (0.8 – 1.8)	2.2 (-3)	P6
2004	24	12	24	330	1.1 (0.5 – 2.5)	1.2 (-2)	P6, P7
2005	21	0	18	350	0.9 (0.5 – 2.0)	3.1 (-4)	P6, P7, P8
2006	23	0	24	310	1.6 (1.1 – 2.3)	3.4 (-1)	P6, P7, P8
2008	13	0	24	310	1.5 (0.8 – 1.9)	1.8 (-0.8)	P2, P7, P8
2009	17	0	24	300	1.1 (0.5 – 1.7)	1.9 (-3)	P2, P7, P8, P9
2010	12	0	24	350	1.1 (0.6 – 2.4)	0.2 (-2)	P2, P7, P8, P9
2011	28	6	24	390	0.8 (0.5 – 1.7)	1.8 (-2)	P2, P6, P8, P9
2012	15	0	24	320	0.8 (0.5 – 1.3)	0.0 (-3)	P2, P6, P8, P9
2013	16	0	24	330	0.9 (0.6 - 1.5)	1.0 (-3)	P2, P6, P8, P9
2014	1	0	36	300	1.7 (1.1 – 4.0)	1.5 (-4)	P1, P2, P9
2015	4	0	24	280	1.0 (0.7 – 1.7)	0.9 (-3)	P1, P2, P9
2016	3	0	24	300	1.0 (0.7 – 1.4)	-0.3 (-3)	P1, P2, P9
2017	9	6	24	310	1.9 (1.0 – 2.6)	-1.3 (-4)	P1, P2, P9
2018	12	8	24	300	1.3 (0.9 – 2.0)	0.0 (-4)	P1, P2, P9

834 \*Daily average of the solar wind velocity

835 \*\*Daily average of the solar wind dynamic pressure and its minimum and maximum in brackets

836 <sup>§</sup>Daily average Bz component of the interplanetary magnetic field and Bz minimum in brackets

837 #POES satellites observed the outer radiation belt

838

839 **Table 3.** Coefficients of the best linear fit of the latitudinal change of the ORB maximum location  
840 with years for various longitudes and energy of electrons

Longitude, deg	Energy, keV	a, deg/year	b, deg
-80	>30	$-0.153 \pm 0.112$	362
-80	>100	$-0.069 \pm 0.097$	192
-80	>300	$-0.057 \pm 0.084$	167
0	>30	$0.021 \pm 0.089$	24
0	>100	$-0.032 \pm 0.063$	129
0	>300	$-0.027 \pm 0.042$	119
100	>30	$-0.265 \pm 0.119$	602
100	>100	$-0.208 \pm 0.106$	486
100	>300	$-0.167 \pm 0.084$	403

841  
842  
843 **Table 4.** Coefficients of the best linear fit of the latitudinal change of the ORB inner edge location  
844 with years for various longitudes and energy of electrons.

Longitude, deg	Energy, keV	a, deg/year	b, deg
-80	>30	$-0.029 \pm 0.065$	106
-80	>100	$-0.021 \pm 0.059$	89
-80	>300	$-0.014 \pm 0.063$	73
0	>30	$0.195 \pm 0.107$	-332
0	>100	$0.241 \pm 0.078$	-424
0	>300	$0.032 \pm 0.069$	-4
100	>30	$-0.183 \pm 0.058$	432
100	>100	$-0.211 \pm 0.037$	487
100	>300	$-0.097 \pm 0.069$	257

845  
846



847 **Figure captions**

848  
849 Figure 1. Solar wind and geomagnetic conditions on 22 to 24 June 2006 (from top to bottom):  
850 solar wind bulk velocity  $V$ ; solar wind dynamic pressure  $P_d$ ; interplanetary magnetic field  
851 magnitude  $B$  (blue dotted curve) and  $B_z$  component (black solid curve); auroral electrojet index  
852  $AE$ ; storm-time  $Dst$  index. The day on 23 June (indicated by vertical red dashed lines) is very quite  
853 in the solar wind and geomagnetic parameters.

854  
855 Figure 2. Geographic maps of energetic electron fluxes with energies  $>300$  keV (a,b),  $>100$  keV  
856 (c,d),  $>30$  keV (e,f) and pitch angles of  $\sim 90^\circ$  observed by POES satellites at height of  $\sim 850$  km in 2  
857 hour vicinity of local noon (left column) on 23 June 2006 and (right column) on 2 June 2016. The  
858 solid wide curve indicates the geomagnetic equator. The outer and inner electron belts and a slot  
859 region between them are clearly seen (excepting of  $>300$  keV electrons), respectively, at high and  
860 middle latitudes in the longitudinal range from  $\sim 90^\circ$  E to  $\sim 80^\circ$  W.

861  
862 Figure 3. Latitudinal profiles of electron fluxes with pitch angles of  $\sim 90^\circ$  observed by POES  
863 satellites during quiet days in different years at height of  $\sim 850$  km in vicinity of local noon at  
864 longitudes around  $100^\circ$  E (red circles),  $0^\circ$  E (blue crosses), and  $80^\circ$  W (black diamonds) for various  
865 energy channels: (a)  $>30$  keV, (b)  $>100$  keV, and (c)  $>300$  keV. Vertical dashed and solid lines  
866 indicate latitudes of the maximum and inner edge of the outer radiation belt, respectively.

867  
868 Figure 4. Geographic latitude of the maximum of the outer radiation belt measured at height of  
869  $\sim 850$  km during geomagnetic quiet days around  $80^\circ$  W (a),  $0^\circ$  E (b), and  $100^\circ$  E (c) for electrons  
870 with energies of  $>30$  keV (red circles),  $>100$  keV (blue crosses), and  $>300$  keV (green triangles).  
871 Dashed curves of corresponding colors show the best linear fit of the latitudinal change of the  
872 maximum location with years (see Table 3). Solid black curves show the latitudinal change  
873 predicted by the IGRF model of corresponding epochs (see details in the text). The grey curve  
874 shows sunspot number (right axis).

875

876 Figure 5. The same as Figure 4 but for the inner edge of the outer radiation belt. [Coefficients of the](#)  
877 [best linear fit are presented in Table 4.](#)

878

879  
880  
881  
882  
883  
884  
885  
886  
887  
888  
889  
890  
891  
892  
893  
894  
895  
896  
897  
898  
899  
900

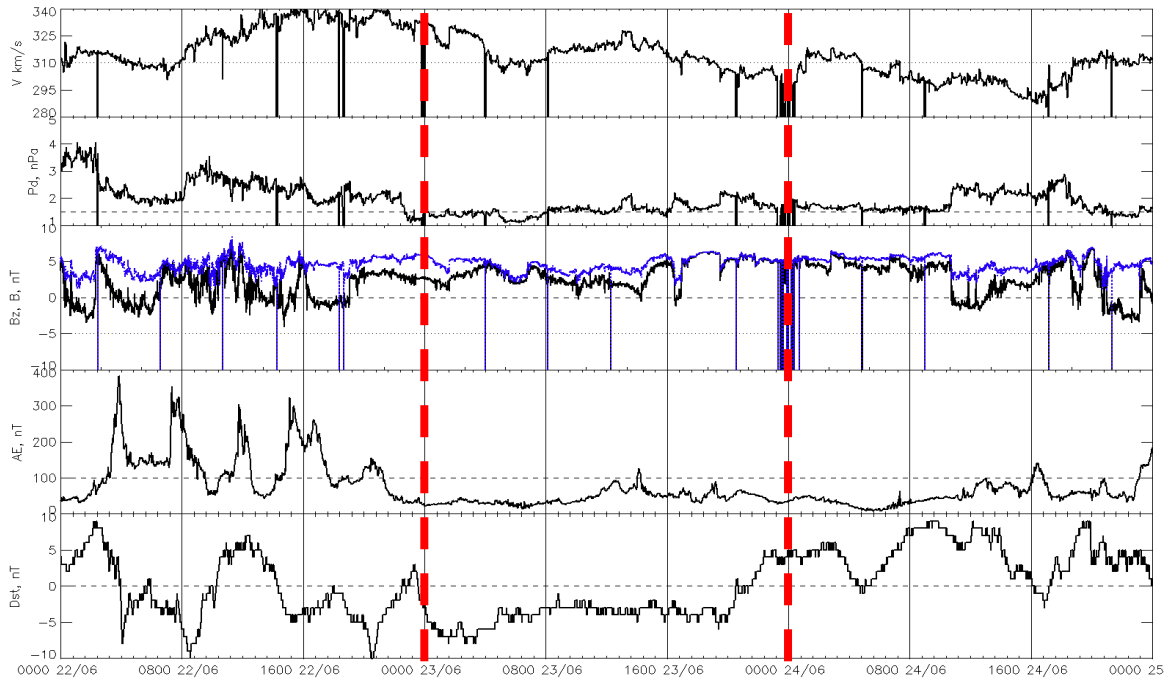
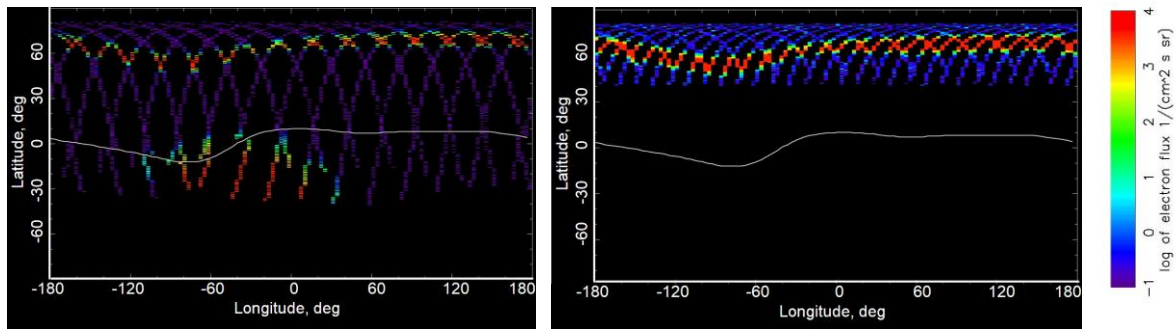


Figure 1. Solar wind and geomagnetic conditions on 22 to 24 June 2006 (from top to bottom): solar wind bulk velocity  $V$ ; solar wind dynamic pressure  $P_d$ ; interplanetary magnetic field magnitude  $B$  (blue dotted curve) and  $B_z$  component (black solid curve); auroral electrojet index  $AE$ ; storm-time  $Dst$  index. The day on 23 June (indicated by vertical red dashed lines) is very quite in the solar wind and geomagnetic parameters.

901  
902

2006

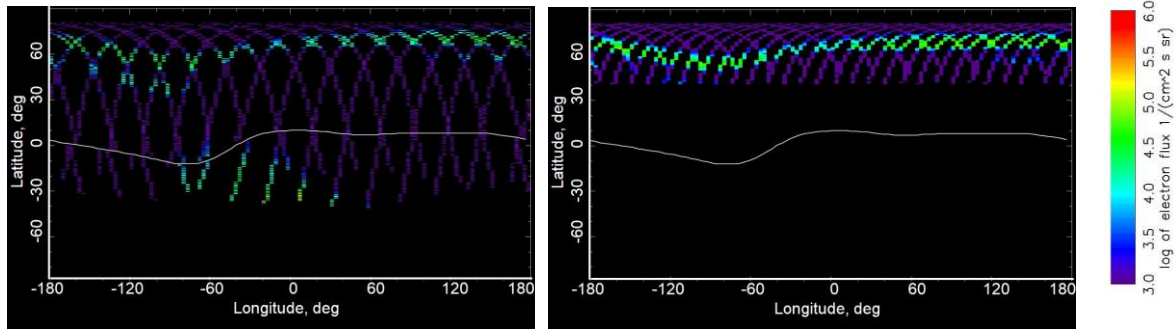
2016



903  
904

a

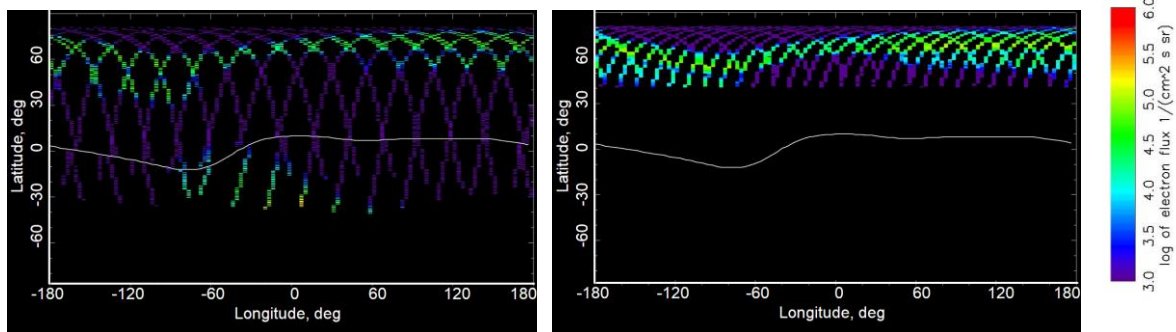
b



905  
906

c

d



907  
908

e

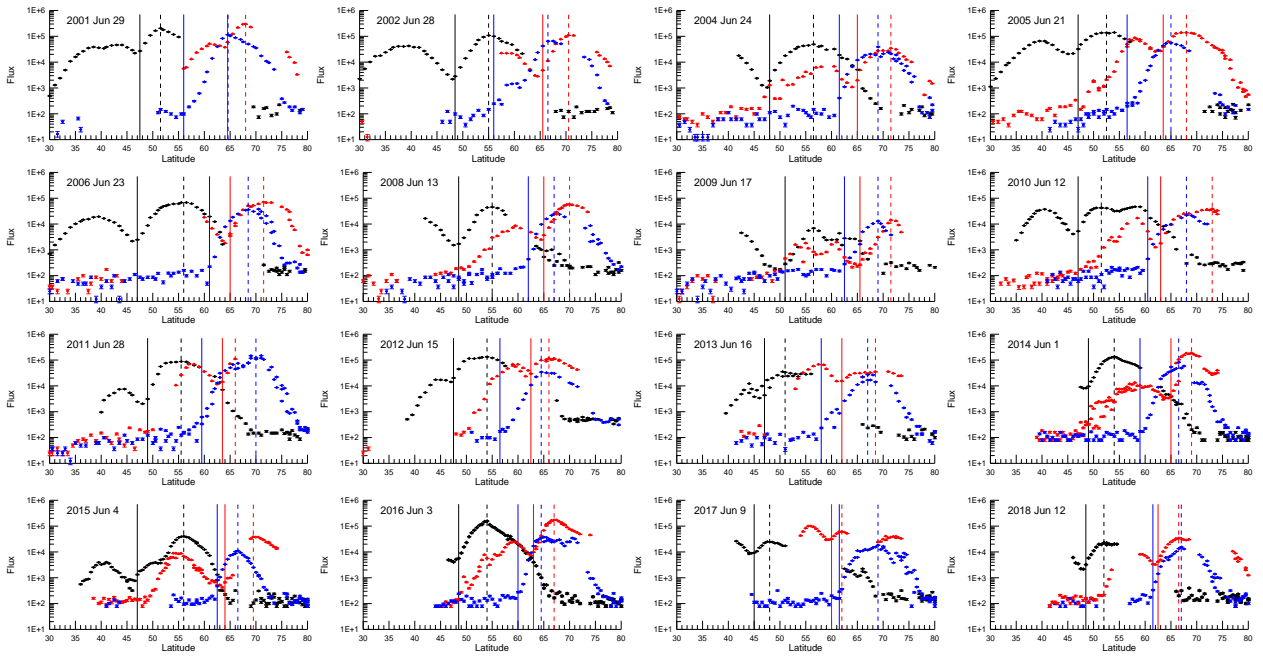
f

909

910 Figure 2. Geographic maps of energetic electron fluxes with energies  $>300$  keV (a,b),  $>100$  keV  
911 (c,d),  $>30$  keV (e,f) and pitch angles of  $\sim 90^\circ$  observed by POES satellites at height of  $\sim 850$  km in 2  
912 hour vicinity of local noon (left column) on 23 June 2006 and (right column) on 3 June 2016. The  
913 solid wide curve indicates the geomagnetic equator. The outer and inner electron belts and a slot  
914 region between them are clearly seen (excepting of  $>100$  keV electrons), respectively, at high and  
915 middle latitudes in the longitudinal range from  $\sim 90^\circ$  E to  $\sim 80^\circ$  W.

916

917

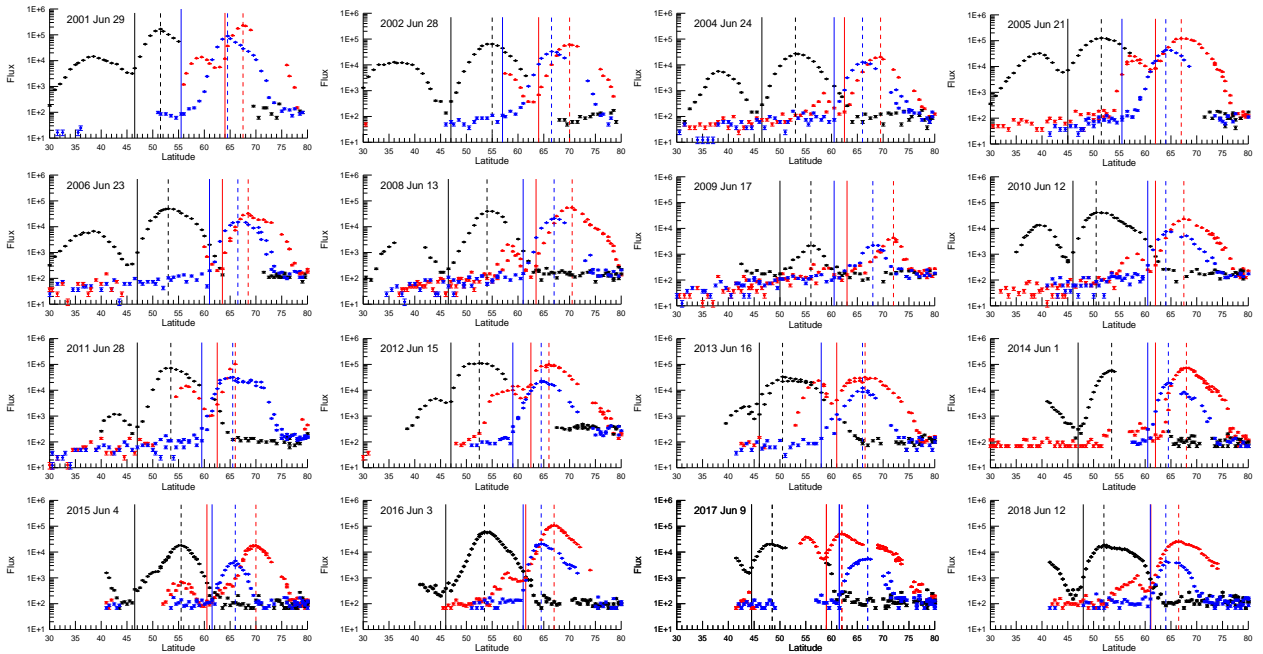


918

919

920

a

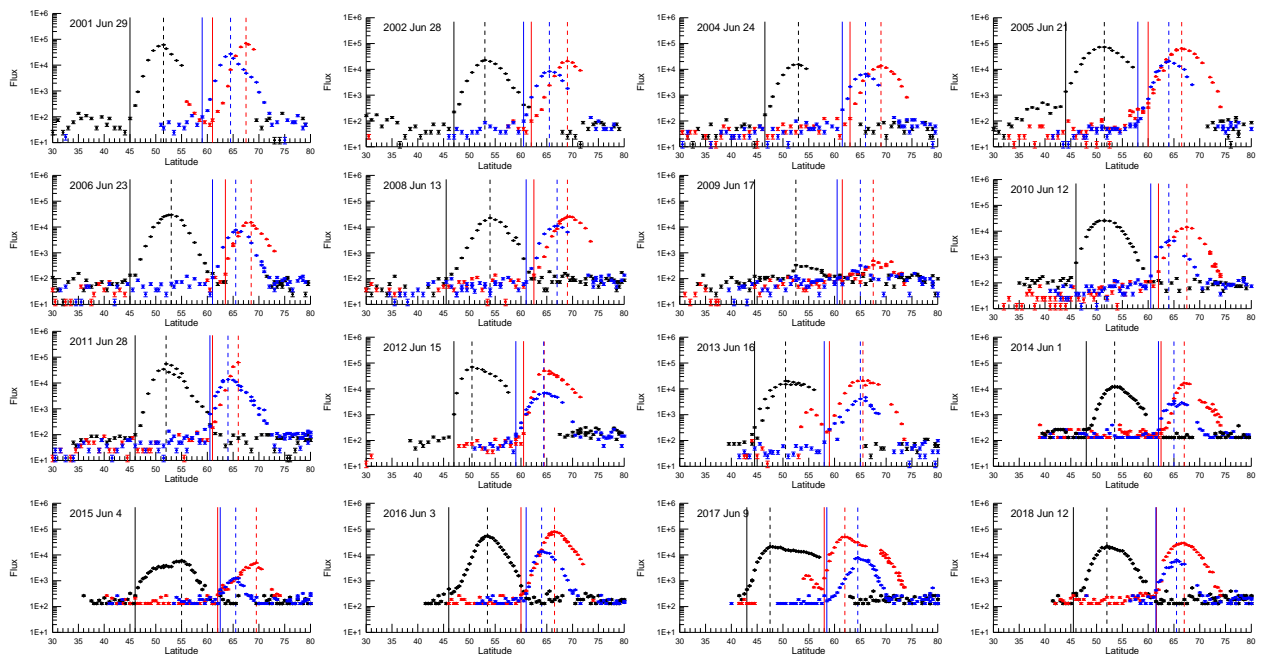


921

922

923

b

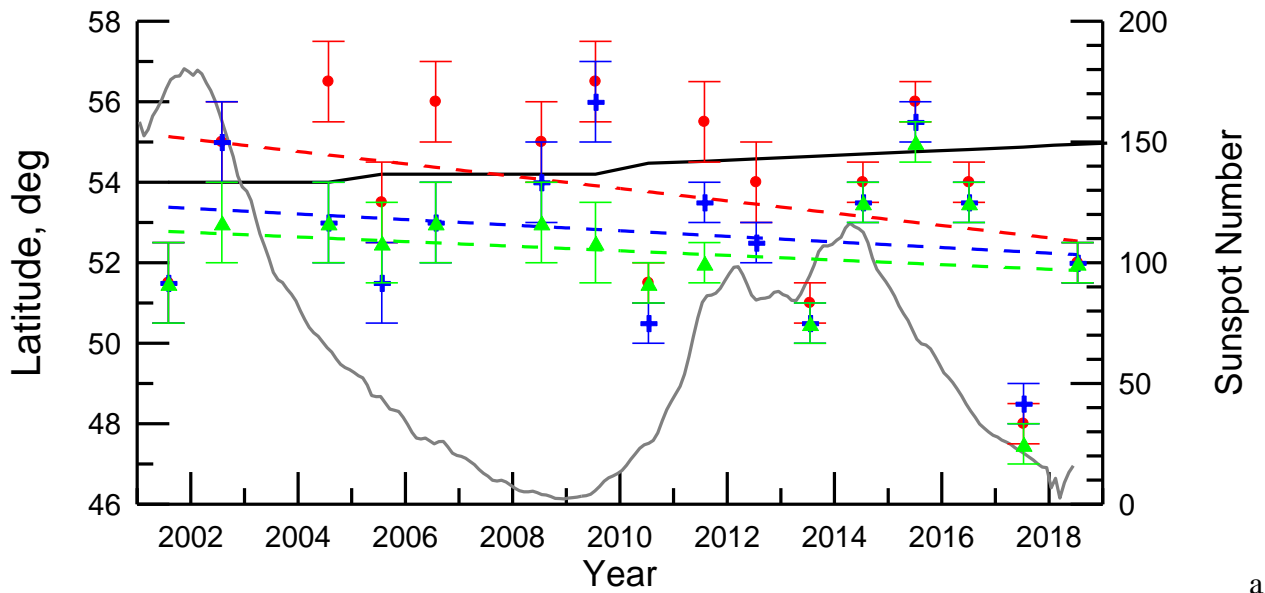


924  
 925  
 926  
 927  
 928  
 929  
 930  
 931

Figure 3. Latitudinal profiles of electron fluxes with pitch angles of  $\sim 90^\circ$  observed by POES satellites during quiet days in different years at height of  $\sim 850$  km in vicinity of local noon at longitudes around  $100^\circ\text{E}$  (red circles),  $0^\circ\text{E}$  (blue crosses), and  $80^\circ\text{W}$  (black diamonds) for various energy channels: (a)  $>30$  keV, (b)  $>100$  keV, and (c)  $>300$  keV. Vertical dashed and solid lines indicate latitudes of the maximum and inner edge of the outer radiation belt, respectively.

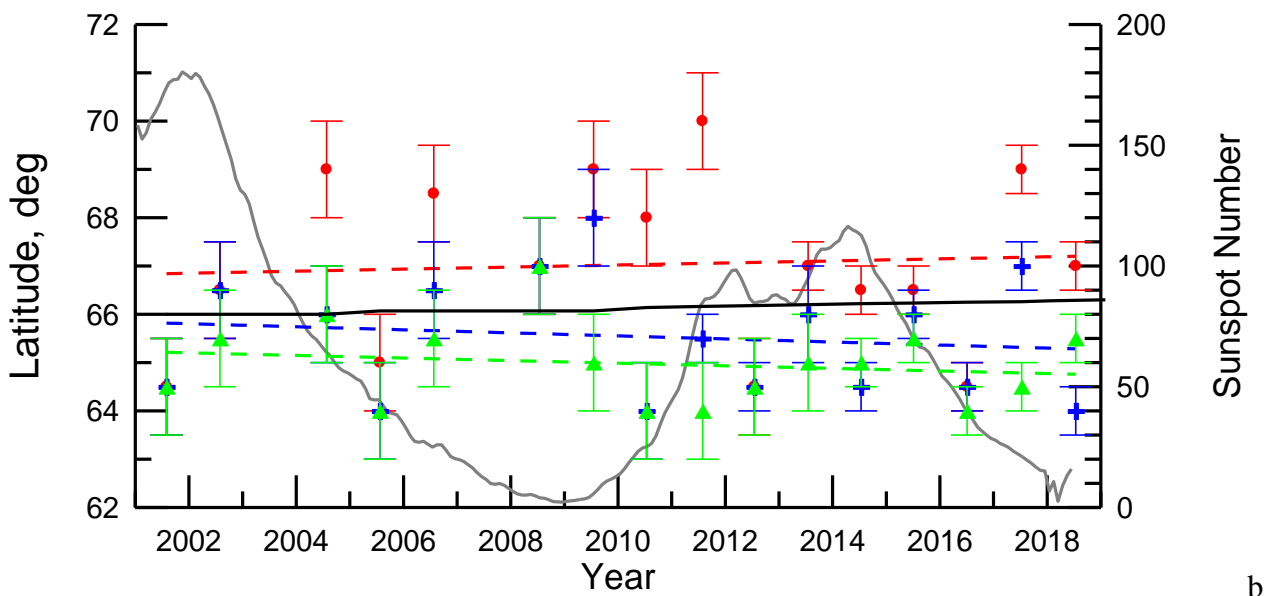
C

932

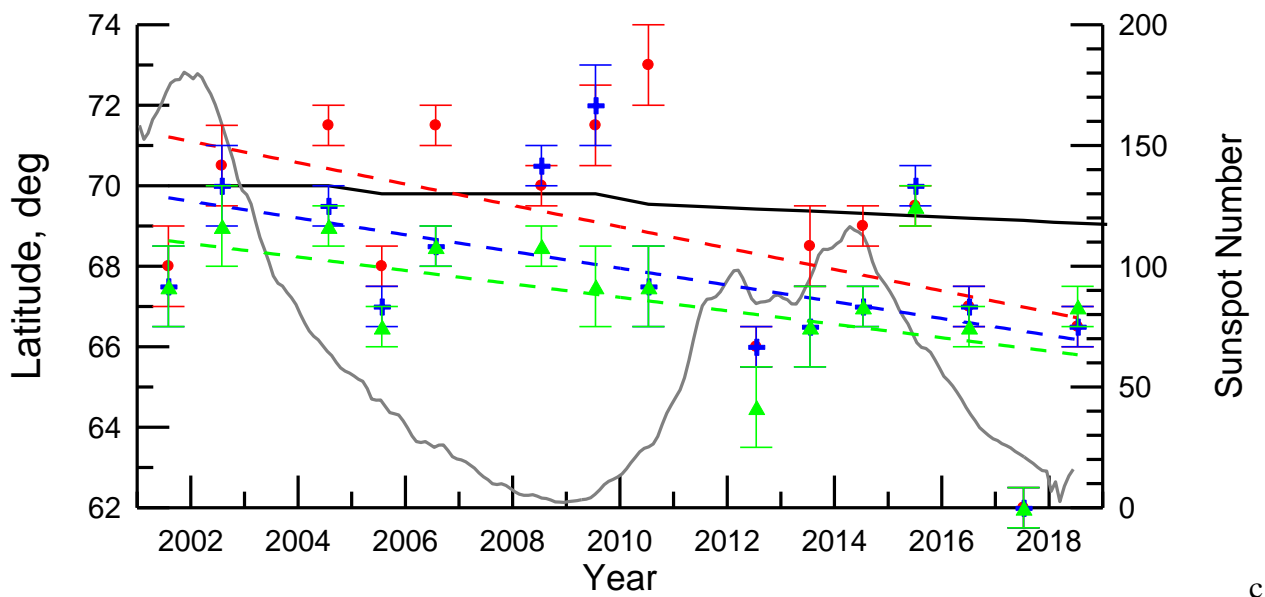


933

934



935



936

a

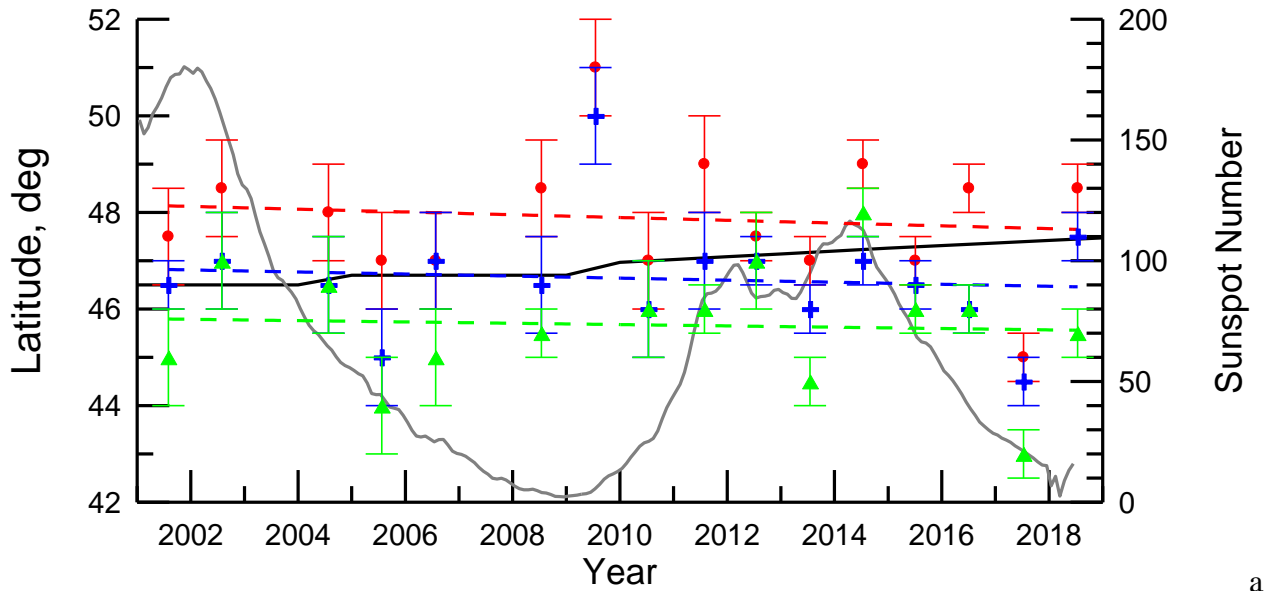
b

c

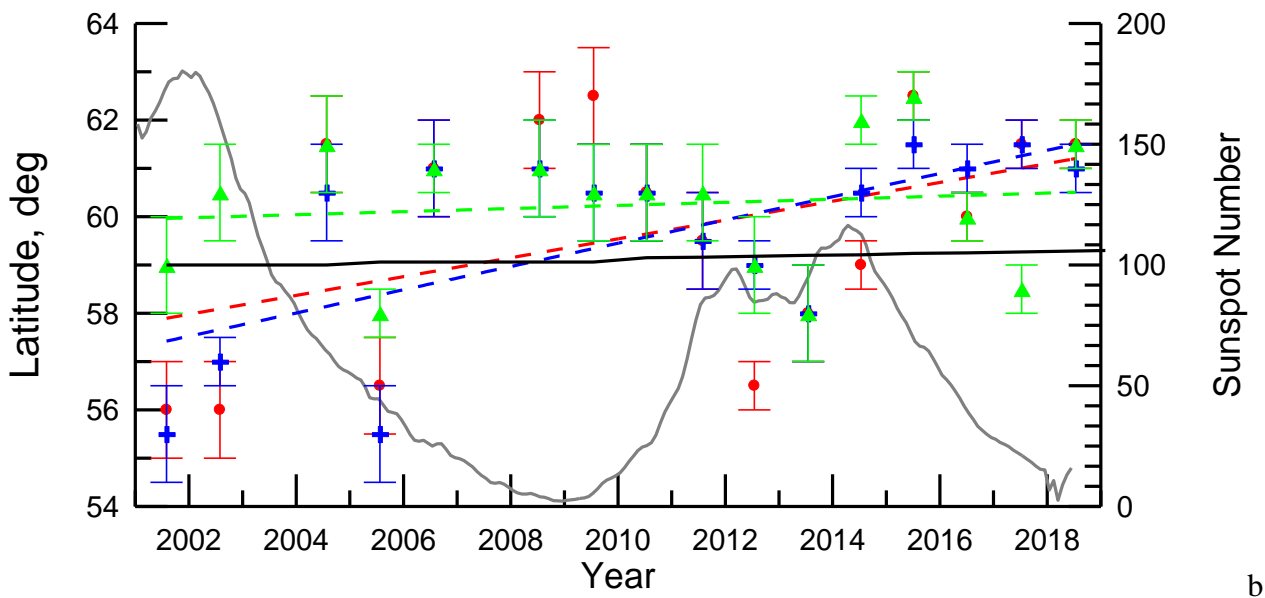
937  
938 Figure 4. Geographic latitude of the maximum of the outer radiation belt measured at height of  
939 ~850 km during geomagnetic quiet days around 80°W (a), 0°E (b), and 100°E (c) for electrons  
940 with energies of >30 keV (red circles), >100 keV (blue crosses), and >300 keV (green triangles).  
941 Dashed curves of corresponding colors show the best linear fit of the latitudinal change of the  
942 maximum location with years (see Table 3). Solid black curves show the latitudinal change  
943 predicted by the IGRF model of corresponding epochs (see details in the text). The grey curve  
944 shows sunspot number (right axis).  
945



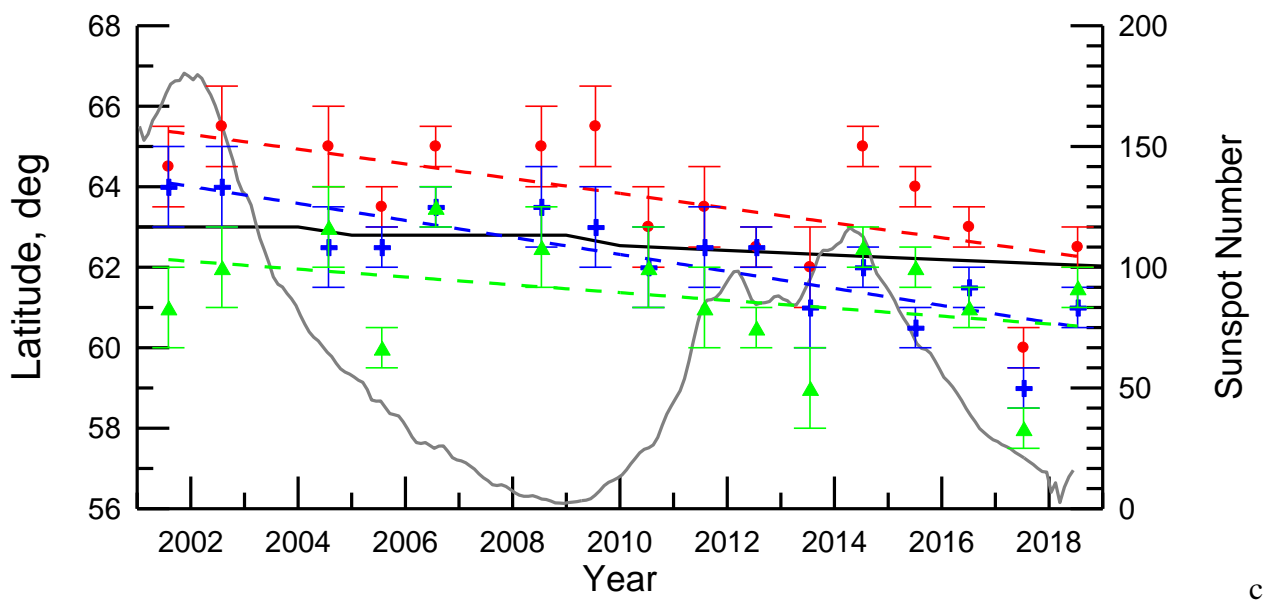
946



947



948



949

950

951 Figure 5. The same as Figure 4 but for the inner edge of the outer radiation belt. [Coefficients of the](#)  
952 [best linear fit are presented in Table 4.](#)  
953